Univ. of Mich.
PHYSICS LIBRARY
Aug 17, 1960

REGISTERED No. M. 3121

PROCEEDINGS
OF THE
INDIAN ACADEMY
OF SCIENCES

VOL. LI] *SECTION A* [No. 5

MAY 1960

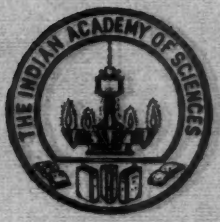

Price Rs. 2 or 3 Sh. *Annual Subscription Rs. 18*

PRINTED AT THE BANGALORE PRESS, BANGALORE CITY, BY T. K. BALAKRISHNAN, SUPERINTENDENT, AND PUBLISHED BY THE INDIAN ACADEMY OF SCIENCES, BANGALORE.

EQUATIONS OF SKY COMPONENTS WITH A "C.I.E. STANDARD OVERCAST SKY"*

By T. N. Seshadri, F.A.Sc.

Received January 9, 1960

Introduction

The sky component due to a given unobstructed window opening, at any point inside a room, in any plane, is defined as the ratio of the intensity of daylight illumination, in that plane, due to the patch of sky visible from that point through the opening, to the simultaneous intensity in a horizontal plane at an external point open to the entire sky vault. This component is independent of the absolute brightness of the sky, but is dependent on its surface distribution.

The general practice for design purposes is to take the worst conditions: and a heavily overcast sky defines the most adverse condition for daylighting. Prior to 1955, a heavily overcast sky was generally assumed to have a uniform distribution of illumination over its surface, and was accordingly called a 'uniform sky'. But measurements carried out by Moon and Spencer (1942) indicated that for a sky entirely covered over with thick dark clouds, the intensity of illumination at any point of the sky was independent of the azimuth and the position of the sun at the time, and varied only with the altitude in accordance with an empirical approximate formula

$$B_\theta = B_z \frac{1 + 2 \sin \theta}{3}$$

where B_z and B_θ are the intensities respectively at the zenith and at an altitude θ. Subsequently, the International Commission on Illumination (C.I.E.) in its sessional meeting at Zurich (1955) defined and recommended for general adoption a "C.I.E. Standard Overcast Sky" in which the intensity varied in strict accordance with the Moon-Spencer formula. Since then, the daylight illumination inside a room is expressed in terms of the intensities, both inside and outside, arising from this Standard Sky only.

As early as 1924 Yamauti derived equations to give the sky components with a "Uniform sky" for vertical rectangular openings. A geometrical

* Paper published with the permission of the Director, Central Building Research Institute, Roorkee.

method was employed to obtain the components at any interior point, in three planes, (*a*) horizontal, (*b*) vertical and perpendicular to the window plane and (*c*) vertical and parallel to the window plane. A need has arisen, since 1955, to derive similar equations for a C.I.E. Standard Overcast Sky. In the absence of such equations, Waldram's diagram (1950), originally constructed for a uniform sky as early as 1923, was modified by Walsh (1959) to suit the standard sky. Rivero (1958) used Yamauti's equations in drawing up his tables for a uniform sky and later modified those values to give tables of sky components for a non-uniform standard sky. Hopkinson, Longmore and Murray Graham (1958) prepared certain Simplified Daylight Tables for glazed openings with a standard sky. But in both an indirect method of computation alone was used to allow for the non-uniform distribution of intensity.

The present paper gives exact trigonometrical equations for direct calculation of sky components due to rectangular windows, both vertical and horizontal, for the C.I.E. Standard Overcast Sky. The same equations will enable direct calculation of sky components due to any rectangular sloping window also, as it can be resolved into a horizontal and a vertical opening. The method adopted is quite general. Yamauti's equations can be derived by the same method. It could also be employed to derive sky component equations arising from an intensity distribution other than that of the standard sky, provided that intensity is a known function of the altitude and independent of the azimuth or *vice-versa*.

GENERAL METHOD OF DERIVATION

In Fig. 1 ABCD is the rectangular vertical window of height h and length l. P is a point on the normal to the window through A and distant d from it. A sphere is described with P as centre and radius d. A projection of ABCD on the spherical surface is AB′C′D′ which is proportional to the patch of the sky visible from P through the window. The intensity at P due that portion of the sky is the same as from AB′C′D′ if the same luminous intensities are assumed at corresponding points.

The values of β, β', γ, γ' the angles subtended at P by the sides AB, DC, AD, BC respectively are given by the following equations:

$$(a)\ \tan \beta = \frac{l}{d}$$

$$(b)\ \tan \gamma = \frac{h}{d}$$

$$(c)\ \tan\beta' = \tan\beta\cos\gamma$$
$$(d)\ \tan\gamma' = \tan\gamma\cos\beta \qquad (1)$$

The following additional relationships between them can also be easily derived:

$$(a)\ \sin\beta' = \sin\beta\cos\gamma'$$
$$(b)\ \sin\gamma' = \sin\gamma\cos\beta'$$
$$(c)\ \cos\beta'\cos\gamma = \cos\gamma'\cos\beta \qquad (2)$$

In Fig. 1, M is a point at azimuth ψ and altitude θ. N_1, N_2, N_3 are the feet of perpendiculars from M on the three mutually perpendicular planes, PAY, PZA, and PZY, respectively. A small element of area of the spherical surface at M between azimuths ψ and $\psi + d\psi$ and altitudes θ and $\theta + d\theta$ is considered. The area of the element is $d^2\cos\theta\, d\theta\, d\psi$. If B is the luminous intensity at M, the intensity of illumination at P due to the element, on a plane perpendicular to PM, is $B\cos\theta\, d\theta\, d\psi$. This expression when multiplied by $\sin\theta$ gives the component of the intensity in the horizontal plane PAY, when multiplied by $\cos N_2MP = \sin MPN_2 = \sin\psi\cos\theta$ (*vide* equation 2 *a*) gives the component on the plane PZA, and when multiplied by $\cos N_3MP = \sin MPN_3 = \cos\psi\cos\theta$ gives the component on the vertical plane PZY. B is a constant for the uniform sky and

$$B = B_\theta = B_z\frac{1 + 2\sin\theta}{3}$$

for the standard sky. The above expressions are integrated over the spherical area AB'C'D' first with respect to θ and then with respect to ψ, between appropriate limits, and later expressed as ratios of the corresponding horizontal intensity due to the total unobstructed hemisphere of the sky, to give the respective sky components.

Horizontal Intensities Due to the Entire Sky Vault

Total horizontal intensity (T_u) at P due to the uniform sky hemisphere is given by

$$T_u = B\int_0^{\pi/2}\int_0^{2\pi}\sin\theta\cos\theta\, d\theta\, d\psi$$
$$= \pi B \text{ (on integration)} \qquad (3)$$

Total horizontal intensity (T_s) at P due to the standard sky hemisphere is given by

$$T_s = \frac{B_z}{3} \int_0^{\pi/2} \int_0^{2\pi} (1 + 2 \sin \theta) \sin \theta \cos \theta \, d\theta \, d\psi$$

$$= \frac{7}{9} \pi B_z \quad \text{(on integration)} \tag{4}$$

SKY COMPONENTS FOR VERTICAL RECTANGULAR WINDOWS

Sky component ($f_{V.H}$) at P on a horizontal plane with a uniform sky is given by

$$f_{V.H} = \frac{B \int_0^{\theta'} \int_0^{\beta} \sin \theta \cos \theta \, d\theta \, d\psi}{T_u} \qquad [T_u \text{ is given by (3)}]$$

where θ' (ref. Fig. 1) is given by $\tan \theta' = \tan \gamma \cos \psi$ (*vide* Equation 1 *d*) where $\tan \gamma$ is a constant. The above equation when integrated over the area AB′C′D′ and simplified gives

$$f_{V.H} = \frac{\beta - \beta' \cos \gamma}{2\pi} \tag{5}$$

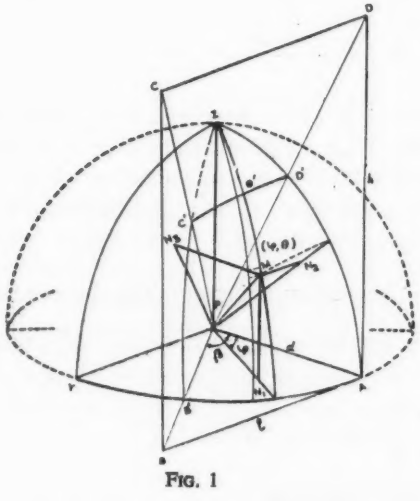

FIG. 1

Sky component ($F_{V.H}$) at P on a horizontal plane with a standard sky is given by

$$F_{v.H} = \frac{\frac{B_z}{3}\int_0^{\theta'}\int_0^{\beta}(1+2\sin\theta)\sin\theta\cos\theta\,d\theta\,d\psi}{T_s} \quad [T_s \text{ is given by (4)}]$$

which on integration and simplification gives

$$F_{v.H} = \frac{3}{14\pi}(\beta - \beta'\cos\gamma) + \frac{2}{7\pi}\sin^{-1}(\sin\beta\sin\gamma) - \frac{1}{7\pi}(\sin 2\gamma\sin\beta'). \tag{6}$$

Similarly expressions for $f_{v.\perp}$ and $F_{v.\perp}$ the sky components on a vertical plane through P perpendicular to the window, for uniform and standard skies respectively, and corresponding expression for $f_{v.\parallel}$ and $F_{v.\parallel}$ the sky components on a vertical plane through P parallel to the window are derived and given below.

$$f_{v.\perp} = \frac{\gamma - \gamma'\cos\beta}{2\pi} \tag{7}$$

$$F_{v.\perp} = \frac{3}{14\pi}(\gamma - \gamma'\cos\beta) + \frac{2}{7\pi}(1 - \cos\beta - \cos\gamma + \cos\beta\cos\gamma') \tag{8}$$

$$f_{v.\parallel} = \frac{\beta'\sin\gamma + \gamma'\sin\beta}{2\pi} \tag{9}$$

$$F_{v.\parallel} = \frac{3}{14\pi}(\beta'\sin\gamma + \gamma'\sin\beta) + \frac{2}{7\pi}(\sin\beta - \sin\beta'\cos^2\gamma) \tag{10}$$

Equations 5, 7 and 9 have been given by Yamauti (1924).

Sky Components for Horizontal Rectangular Windows

Figure 2 gives the diagram of a horizontal rectangular opening ABCD. AB'C'D' is its projection on the surface of a sphere described with P as centre and radius d, and is proportional to the patch of the sky visible through the window from P. β, β', γ, γ' are again taken as the angles subtended by the sides AB, DC, AD and BC respectively. Their values will be given by the same equations (1) and (2). The value of the angle α (ref. to Fig. 2) is given by the equation

$$\tan\alpha = \frac{\tan\gamma}{\tan\beta}. \tag{11}$$

For any element of area at M included between azimuths ψ and $\psi + d\psi$ and altitudes θ and $\theta + d\theta$ the expression $B_\theta \cos\theta\,d\theta\,d\psi$ where B_θ is a

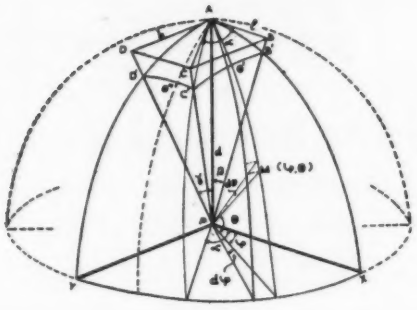

FIG. 2

constant for the uniform sky or equal to $B_z(1 + 2 \sin \theta)/3$ for the standard sky gives the intensity at P in a plane normal to the line joining P with the element M. This expression is multiplied by the factors $\sin \theta$, $\sin \psi \cos \theta$, or $\cos \psi \cos \theta$ as before to give the components of intensity at P in the horizontal plane, β plane (APX), and γ plane (APY) respectively. The integrations however are carried out in two stages, between limits $\pi/2$ and θ' for θ, and α and 0 for ψ in the first stage, and between limits $\pi/2$ and θ'' for θ, and $\pi/2$ and α for ψ in the second stage, where θ' and θ'' are functions of ψ given by the equations

$$\tan \theta' = \cot \beta \cos \psi \tag{12}$$

$$\tan \theta'' = \cot \gamma \sin \psi \tag{13}$$

The two integrated values are added together and expressed as a ratio of the horizontal intensity due to the total hemisphere of the sky T_u for the uniform sky or T_s for the standard sky (Equations 3 and 4) to give the respective sky components. The following equations can then be derived, where $f_{H.H}$, $f_{H.\beta}$ and $f_{H.\gamma}$ are the sky components with an uniform sky and $F_{H.H}$, $F_{H.\beta}$ and $F_{H.\gamma}$ are the sky components with a standard overcast sky, in the horizontal, β and γ planes respectively.

With uniform sky

$$f_{H.H} = \frac{1}{2\pi}(\beta' \sin \gamma + \gamma' \sin \beta) \tag{14}$$

$$f_{H.\beta} = \frac{1}{2\pi}(\beta - \beta' \cos \gamma) \tag{15}$$

$$f_{H.\gamma} = \frac{1}{2\pi}(\gamma - \gamma' \cos \beta). \tag{16}$$

With C.I.E. Standard overcast sky

$$F_{H.H} = \frac{3}{14\pi}(\beta' \sin\gamma + \gamma' \sin\beta) + \frac{1}{7} + \frac{1}{7\pi}(\sin 2\beta \sin\gamma' + \sin 2\gamma \sin\beta') - \frac{2}{7\pi}\sin^{-1}(\sin\alpha \cos\beta) - \frac{2}{7\pi}\sin^{-1}(\cos\alpha \cos\gamma) \quad (17)$$

$$F_{H.\beta} = \frac{3}{14\pi}(\beta - \beta' \cos\gamma) + \frac{2}{7\pi}(\sin\beta - \sin\beta' \cos^2\gamma) \quad (18)$$

$$F_{H.\gamma} = \frac{3}{14\pi}(\gamma - \gamma' \cos\beta) + \frac{2}{7\pi}(\sin\gamma - \sin\gamma' \cos^2\beta). \quad (19)$$

Equations (14), (15) and (16) can be surmised from Yamauti's equations for vertical windows. One can also understand how equation (19) can be readily obtained from equation (18) by merely interchanging β with γ and β' with γ'.

In the equations derived above the angles are obviously to be expressed in radian measure. It however facilitates calculations to express the angles in degrees. Moreover it is usual to express the sky components as percentages. The equations modified accordingly are given below for sky components with the C.I.E. standard overcast sky.

Vertical windows:

$$\%F_{V.H} = \frac{\beta - \beta' \cos\gamma}{8{\cdot}4} + \frac{\sin^{-1}(\sin\beta \sin\gamma)}{6{\cdot}3} - 4{\cdot}547 \sin 2\gamma \sin\beta' \quad (20)$$

$$\%F_{V.\perp} = \frac{\gamma - \gamma' \cos\beta}{8{\cdot}4} + 9{\cdot}095\,(1 - \cos\beta - \cos\gamma + \cos\beta \cos\gamma') \quad (21)$$

$$\%F_{V.\parallel} = \frac{\beta' \sin\gamma + \gamma' \sin\beta}{8{\cdot}4} + 9{\cdot}095\,(\sin\beta - \sin\beta' \cos^2\gamma). \quad (22)$$

Horizontal windows:

$$\%F_{H.H} = \frac{\beta' \sin\gamma + \gamma' \sin\beta}{8{\cdot}4} + 14{\cdot}286 + 4{\cdot}547\,(\sin 2\beta \sin\gamma' + \sin 2\gamma \sin\beta') - \frac{\sin^{-1}(\sin\alpha \cos\beta) + \sin^{-1}(\cos\alpha \cos\gamma)}{6{\cdot}3} \quad (23)$$

$$\%F_{H.\beta} = \frac{\beta - \beta' \cos\gamma}{8{\cdot}4} + 9{\cdot}095\,(\sin\beta - \sin\beta' \cos^2\gamma) \tag{24}$$

$$\%F_{H.\gamma} = \frac{\gamma - \gamma' \cos\beta}{8{\cdot}4} + 9{\cdot}095\,(\sin\gamma - \sin\gamma' \cos^2\beta). \tag{25}$$

[The angles in equations (20) to (25) are expressed in degrees.]

The first terms in the above equations, with 3·6 replacing 8·4, gives the corresponding sky components with a uniform sky.

The above equations for a point P at infinity get reduced each to a value zero. When the point P coincides with A, *i.e.*, when

$$\beta = \gamma = \beta' + \gamma' = \frac{\pi}{2} \quad \text{or} \quad 90°$$

the horizontal components get reduced each to a value 25%. The components in the vertical planes get reduced each to a value

$$\left(\frac{3}{28} + \frac{2}{7\pi}\right) 100\% = 19{\cdot}8\% \text{ (about).}$$

This later value can be easily derived as the sky component over either of the two mutually perpendicular vertical planes for a quarter hemisphere of a standard sky enclosed between them. For a uniform sky all values will be 25% when P coincides with A.

The values calculated from these equations tally approximately with those given in Rivero's tables, indicating thereby the care and accuracy with which the latter values have been computed though employing an indirect method.

The equations given above are derived for a point P on the perpendicular through one corner of the window. If the point is not so situated and when the sill is above the point, the rectangular window should first be considered extended up to the foot of the perpendicular from the point on the plane of the window. The additional area can be considered as an algebraic sum of three rectangular areas each with one of their corners at the foot of the perpendicular from the point. The total sky component for the additional area, which can now be calculated, is then deducted from the component for the extended window, to give the component for the actual window. When the sill of the window is below the horizontal plane through the point, the portion of the window below that plane is neglected. It is thus possible to enlarge the utility of the equations to the general case of any point inside.

Glazing Correction

The loss in transmission through glass at various angles of incidence can be calculated from the Fresnel's equation. The loss is about 4% at normal incidence from each surface of the pane. At other angles of incidence the loss is more. Rivero (1958) has given the following empirical formula for the transmission factors at different angles of incidence.

$$\tau = c\,(1 + \sin^3\theta)\cos\theta, \quad \text{where} \quad c = 0{\cdot}81 \text{ (about)}.$$

This formula agrees with the theoretical curve fairly well, and is of a form convenient to adopt as an additional factor in the equations to be integrated. Sky components for glazed windows can then be easily derived using the general method adopted in this paper. Such equations are however not given here, as they are not likely to be of much practical significance. The glazing losses increase rapidly with the degree of dirtiness of the glass panes, depending on the period they are left uncleaned, the density of atmospheric dust at the locality, the inclination and orientation of the windows, etc. Such losses can be estimated only approximately and may amount to as much as 50% and more under bad conditions. There does not appear therefore to be any justification to calculate it with precision taking into consideration only the relatively minor variation of transmission factor with angle of incidence. Quite satisfactory results would be obtained for all practical purposes if the sky components for unglazed openings are reduced by a value 10 to 20% to allow for glazing losses, provided the glass panes are tolerably clean.

Summary

Rigorous trigonometrical equations for calculating directly the sky components at any point due to a C.I.E. Standard Overcast Sky for both vertical and horizontal rectangular unglazed windows are derived and presented. The equations, when suitably combined, can also be used for any sloping window. The general method adopted can be used to derive similar equations for a sky with any intensity distribution, provided that intensity is a function of altitude alone and independent of azimuth or *vice-versa*.

References

C.I.E. Proc., 1955, **2**.

Hopkinson, R. G., Longmore, J. and Murray Graham, A. *Simplified Daylight Tables*, 1958, H.M.S.O., London.

Moon, P. and Spencer, D. E. .. *Illuminating Engineering*, 1942, **37**, 707–26.

Rivero, R. .. *Illuminacion Natural*, 1958, Translated from Spanish by R. G. Hopkinson, B.R.S., L.C. No. 860, 1959.

Waldram, P. J. .. *A Measuring Diagram for Daylight Illumination*, B.T. Batsford, Ltd., London, 1950.

Walsh, J. W. T. .. *Architects Journal*, 1959, **129**, 440–42.

Yamauti, Z. .. "Geometrical Calculation of Illumination," *Electrot. Lab. Tokyo Researches*, 1924, **148**.

PROTON EMISSION FROM NUCLEI DUE TO NEUTRON INTERACTIONS

By G. S. Mani and K. G. Nair*

(*Atomic Energy Establishment, Trombay, Bombay*)

Received September 30, 1959

(Communicated by Dr. B. V. Thosar, F.A.SC.)

Abstract

The energy spectra of protons emitted in neutron bombardment of Al^{27} is analysed in terms of the statistical model and volume direct interaction. It is found that the diffuseness of the nuclear potential or the form of level density used does not alter the shape of the energy spectra very much. The available experimental data agree fairly well with theory. The contribution of direct interaction is seen to be small and hence does not alter the general shape of the spectra. The direct interaction cross-section obtained from the measurements of the angular distribution in the case of iron and copper agree reasonably well with theory.

Introduction

In recent years a large number of experiments[1, 2, 3] have indicated the inadequacy of the statistical theory in explaining the data. The two assumptions of the statistical theory are (i) an intermediary compound system is formed which decays after a relatively long time, (ii) the contribution from the several overlapping levels in the highly excited compound system have random phases so that interference effects can be neglected. These assumptions lead to symmetry about 90° in the angular distribution and linear dependence of the spectra of the emitted particles to the level density of the compound or the residual nucleus. The angular distribution would further be isotropic if the density of levels of total angular momentum J follows the $(2J + 1)$ law.[4]

Most of the experimental results indicate that (i) the angular distribution is not symmetric about 90° and is mainly peaked in the forward angles. This anisotropy increases with increasing energy of the emitted particle, corresponding to the low-lying states of the residual nucleus. (ii) The high

* Tata Institute of Fundamental Research, Apollo Pier Road, Bombay 1.

energy region of the spectra is much larger than predicted by the level density. Also the spectra exhibit peaks in the high energy region which correspond to the discrete low-lying levels of the residual nucleus. There are some indications of the preponderance of low energy protons in (n, p) reactions.[5]

The angular distribution of the emitted particles which leave the residual nucleus in discrete low-lying levels has been explained by the surface direct interaction which closely resembles stripping and pick-up reactions.[6] Unfortunately the theory is at present unable to predict absolute cross-sections.

The general increase in the high energy part of the spectra may be due to any one of the following reasons: (i) Modification of level density formula taking into account of the effective mass of nucleons inside the nucleus as shown by the optical model.[7] (ii) Volume direct interaction.[8–10]. (iii) Interactions in which a large number of nucleons take part in the reaction like spot heating of the nucleus and collective excitation.

The preponderance of low energy protons in (n, p) reactions may be due to the diffuseness of the nuclear potential,[11] modification of the level density formula taking into account the effect due to pairing energy as suggested by Newton[12] and contributions from reactions like (n, np) due to compound as well as direct processes.

In this paper we shall investigate the effects of these various factors on the shape of the energy spectra of protons emitted from Al^{27} nucleus bombarded with neutrons. It has been pointed out[13] that volume direct interaction does not contribute appreciably to the total direct interaction cross-section, especially in heavy nuclei, due to surface reflection and attenuation in nuclear volume. The effects of surface reflection and attenuation would be predominant if $R \gg \lambda$ where R is the nuclear radius and λ is the mean free path of nucleons in nuclear matter. Since $\lambda \sim 3{\cdot}3 \times 10^{-13}$ cm. for the energy region under consideration,[9,14] the above effects would not appreciably diminish the volume direct interaction cross-section for nuclei with mass number $A \sim 60$. To test this assumption, the experimental value of the direct interaction cross-section for iron and copper has been compared with the theory of volume direct interaction.

THEORY

Neutron bombardment of Al^{27} would yield the following reactions:

1. (n, p) and (n, pn) due to compound process.
2. (n, n'), $(n, n'\ n)$ and $(n, n'\ p)$ due to compound process.

3. (n, p) and (n, pn) due to direct process. In the case of (n, pn) the neutron can be directly ejected simultaneously with the proton or can boil off the residual nucleus.

4. (n, n'), $(n, n'\ n)$ and $(n, n'\ p)$ due to direct processes. In the case of $(n, n'\ n)$ and $(n, n'\ p)$ the second neutron or proton can be simultaneously ejected with the first neutron or can boil off the residual nucleus.

5. (n, α) and $(n, \alpha n)$ reactions.

Reactions like (n, γ), (n, d), (n, t), $(n, 2p)$ are neglected either because their cross-sections for energies of incident neutrons up to 20 MeV are negligible[15] or because they are not energetically possible.

The spectra of protons from (n, p) and (n, pn) reactions are given in the statistical theory by Blatt and Weisskopf.[16] This expression is valid only when the level density follows the $(2J+1)$ law.

$$n(\epsilon)\, d\epsilon = \frac{\sigma_I \epsilon \sigma_C(\epsilon)\, \omega(\epsilon_0 - \epsilon)\, d\epsilon}{\sum_\nu F_\nu} \tag{1}$$

where σ_I is the cross-section for the formation of the compound nucleus due to the interaction of the target nucleus with incident neutron, $\sigma_C(\epsilon)$ is the cross-section for the formation of the compound nucleus due to the interaction of the residual nucleus in the excited state with the emitted proton of energy ϵ, ϵ_0 is the maximum possible energy for the emitted proton and involves the incident neutron energy and Q value of the reaction. $\omega(\epsilon^*)$ is the level density of the residual nucleus at the excitation energy, $\epsilon^* = \epsilon_0 - \epsilon$, $\sum_\nu F_\nu$ is the total probability for the compound system to decay into the various channels ν. Since (n, pp) for the energies under consideration is very improbable due to Coulomb barrier, we have assumed that only a neutron can boil off the residual nucleus. For the energies of interest we have assumed that simultaneous evaporation of two or more particles from the compound nucleus is improbable. As will be seen later the experimental data seem to support this approximation.

The various cross-sections have been evaluated using the following two formulæ for the level density:

$$\omega(\epsilon) = C \exp.\ [2a^{\frac{1}{2}} \epsilon^{\frac{1}{2}}] \tag{2}$$

$$\omega(\epsilon) = C \exp.\ [2a^{\frac{1}{2}} (\epsilon - \Delta\epsilon)^{\frac{1}{2}}] \tag{3}$$

where 'a' is a measure of the nuclear temperature and we have assumed it to be the same for all nuclei under consideration. 'C' is a constant which

may vary widely from nucleus to nucleus and in effect it determines the level density for the particular nucleus. $\Delta\epsilon$ is the pairing energy for the nucleus under consideration and has been evaluated by Cameron.[17]

Since it is very difficult to estimate the value of the constant C due to our lack of knowledge of level density in nuclei, we have eliminated it from the equations by using the experimental value of the total (n, p) cross-section.

$$[\sigma(n,p)]_{\text{comp.}} = \frac{\sigma_1 C \int_{\epsilon_0 - B_n}^{\epsilon_0} \epsilon\sigma_c(\epsilon) \exp.(2a^{\frac{1}{2}}\epsilon'^{\frac{1}{2}})\, d\epsilon}{\sum_{\nu} F_\nu} \tag{4}$$

where B_n is the binding energy of the last neutron in the residual nucleus and $\epsilon' = (\epsilon_0 - \epsilon)$ or $\epsilon' = (\epsilon_0 - \epsilon - \Delta\epsilon)$ depending on the level density formula used. $[\sigma(n,p)]_{\text{comp.}}$ is the total cross-section for the (n, p) reaction going through the compound process. From (1) and (4) we obtain

$$n(\epsilon)\, d\epsilon = \frac{[\sigma(n,p)]_{\text{comp.}}\, \epsilon\sigma_c(\epsilon) \exp.[2a^{\frac{1}{2}}\epsilon'^{\frac{1}{2}}]\, d\epsilon}{\int_{\epsilon_0 - B_n}^{\epsilon_0} \epsilon\sigma_c(\epsilon) \exp\ [2a^{\frac{1}{2}}\epsilon'^{\frac{1}{2}}]\, d\epsilon} \tag{5}$$

whieh is independant of the constant C. $[\sigma(n,p)]_{\text{comp.}}$ is obtained from the relation

$$[\sigma(n,p]_{\text{comp.}} = [\sigma(n,p)]_{\text{exp.}} - [\sigma(n,p)]_{\text{dir.}} \tag{6}$$

where $[\sigma(n,p)]_{\text{exp.}}$ is the experimental value for the total (n, p) cross-section and $[\sigma(n,p)]_{\text{dir.}}$ is the total (n, p) cross-section due to direct interaction and is evaluated later [*see* eq. (14)].

The spectra of protons due to (n, np) reaction proceeding through the compound system is obtained as follows:

Let $N(\epsilon_n)\, d\epsilon_n$ be the spectra of neutrons from the (n, n') reaction. Let B_n and B_p be the binding energies of the last neutron and proton respectively of the residual nucleus. No further proton emission is possible if $\epsilon_n > (\epsilon_{0n} - B_p)$ where ϵ_{0n} is the maximum energy with which neutrons can be emitted in the (n, n') reaction. Similarly no neutron emission from the residual nucleus is possible if $\epsilon_n > (\epsilon_{0n} - B_n)$. Let $N(\epsilon_n, \epsilon_n')\, d\epsilon_n d\epsilon_n'$ be the number of secondary neutrons emitted in the range ϵ_n' and $\epsilon_n' + d\epsilon_n'$ after the emission of $N(\epsilon_n)\, d\epsilon_n$ primary neutrons. Similarly let $N(\epsilon_n, \epsilon_p)\, d\epsilon_n d\epsilon_p$ be the distribution function for secondary protons. From the statistical theory we have

$$N(\epsilon_n, \epsilon_n')\, d\epsilon_n d\epsilon_n' = C_{n'}\, K(\epsilon_n)\, \sigma_c(\epsilon_n') \exp.[2a^{\frac{1}{2}}\epsilon_n''^{\frac{1}{2}})\, d\epsilon_n' \tag{7}$$

$$N(\epsilon_n, \epsilon_p)\, d\epsilon_n d\epsilon_p = C_p\, K(\epsilon_n)\, \sigma_c(\epsilon_p) \exp.(2a^{\frac{1}{2}}\epsilon_p''^{\frac{1}{2}})\, d\epsilon_p \tag{8}$$

where C_n' and C_p are the C-values of the corresponding residual nucleus after secondary emission. $K(\epsilon_n)$ is a constant of proportionality. ϵ_n'' and ϵ_p'' denote the excitation energies of the corresponding residual nuclei. Since we assume that no other mode of decay is possible [the $(n, n'\ \alpha)$ is neglected since the alpha particle, which has a relatively low energy, would have to overcome a much higher Coulomb barrier],

$$N(\epsilon_n)\, d\epsilon_n = C_n' K(\epsilon_n) \int_0^{\epsilon_n'^{\max.}} \epsilon_n' \sigma_c(\epsilon_n') \exp.\,[2a^{\frac{1}{2}} \epsilon_n''^{\frac{1}{2}}]\, d\epsilon_n' + C_p K(\epsilon_n) \int_0^{\epsilon_p \max.} \epsilon_p \sigma_c(\epsilon_p) \exp.\,[2a^{\frac{1}{2}} \epsilon_p''^{\frac{1}{2}}]\, d\epsilon_p. \tag{9}$$

Hence

$$K(\epsilon_n) = \frac{N(\epsilon_n)\, d\epsilon_n}{C_n' \int_0^{\epsilon_n'^{\max.}} \epsilon_n' \sigma_c(\epsilon_n') \exp.\,[2a^{\frac{1}{2}} \epsilon_n''^{\frac{1}{2}}]\, d\epsilon_n' + C_p \int_0^{\epsilon_p \max.} \epsilon_p \sigma_c(\epsilon_p) \exp.\,[2a^{\frac{1}{2}} \epsilon_p''^{\frac{1}{2}}]\, d\epsilon_p} \tag{10}$$

where

$$\epsilon_{n\,\max.}' = \epsilon_{0n} - \epsilon_n - B_n.$$
$$\epsilon_{p\,\max.} = \epsilon_{0n} - \epsilon_n - B_p. \tag{11}$$

Hence if $N(\epsilon_n)\, d\epsilon_n$ and C_n'/C_p are known, the (n, np) spectrum is obtained from equation (8). The total $(n, 2n)$ cross-section in Al^{27} cannot easily be determined since the ground state of Al^{26} has a very long half-life, $(8 \cdot 10^5 y)$.[15] Hence we cannot eliminate $C_{n'}/C_p$ from the above equation. For Al^{27}, the $(n, 2n)$ reaction yields Al^{26} which is an odd-odd nucleus while the (n, np) reaction yields the even-even nucleus Mg^{26}. Following the prescription suggested by Brown and Muirhead,[10] we have assumed $C_{n'}/C_p = 10$. This assumption will not alter the spectra very much since the $(n, 2n)$ contribution in the energy region of interest is small, the threshold of the reaction being around 13 MeV.

The (n, n') spectrum can be obtained in the same way as the (n, p) spectrum and we get

$$N(\epsilon_n)\, d\epsilon_n = \frac{[\sigma(n, n')]_{\text{comp.}}\, \epsilon_n \sigma_c(\epsilon_n) \exp.\,(2a^{\frac{1}{2}} \epsilon_n''^{\frac{1}{2}})\, d\epsilon_n}{\int_0^{\epsilon_{0n}} \epsilon_n \sigma_c(\epsilon_n) \exp.\,[2a^{\frac{1}{2}} \epsilon_n''^{\frac{1}{2}}]\, d\epsilon_n} \tag{12}$$

where the lower limit of the integral is taken as zero since we include all reactions of the type $(n, n'x)$.

$$[\sigma(n, n')]_{\text{comp.}} = \sigma_{ne} - [\sigma(n, p) + \sigma(n, pn)]_{\text{comp.}} - [\sigma(n, p) + \sigma(n, pn)]_{\text{dir.}} - [\sigma(n, \alpha) + \sigma(n, \alpha n)]_{\text{exp.}} - [\sigma(n, n')_{\text{dir.}}] \quad (13)$$

where σ_{ne} is the experimentally measured non-elastic cross-section. $[\sigma(n, p) + \sigma(n, pn)]_{\text{comp.}}$ is obtained from equation (5). $[\sigma(n, p) + \sigma(n, pn)]_{\text{dir.}}$ and $[\sigma(n, n')]_{\text{dir.}}$ from equations (14) – (16). $[\sigma(n, \alpha) + \sigma(n, \alpha n)]_{\text{comp.}}$ has been evaluated from the experimental value of $\sigma(n, \alpha)$ following the same procedure as in the case of the $(n, p) + (n, pn)$ reaction. We have chosen the total non-elastic cross-section since the (n, n') cross-section is not known for these energies. Thus from (10), (11), (12) and (8) we can evaluate the proton spectrum due to (n, np) reaction.

The contribution of the direct interaction process to these various reactions has been evaluated as follows. The nucleus is assumed to be composed of two non-interacting Fermi gases and the collisions of the incident neutrons with individual nucleons in the nucleus give rise to these reactions. These collisions are considered to be free nucleon-nucleon collisions except for the restriction imposed on their final momentum states by the Pauli exclusion principle. We shall not give below the complete derivation of the various cross-sections but only quote the final results since these have been derived in detail by Hayakawa *et al.*[9] and by Brown and Muirhead.[10] The neutron-nucleon collision inside the nucleus may yield any one of the following reactions:

(1) $n - p$ collisions with both particles simultaneously ejected.

(2) $n - p$ collisions in which only the protons are emitted.

In case (1) the final nucleus may boil off a neutron, thus yielding the $(n, 2np)$ reaction. For the energy region under consideration this is not energetically possible. In case (2) the final nucleus may similarly boil off a neutron yielding the (n, pn) reaction. Since we disregard the (n, pp) reaction, calculation of the (n, p) would automatically yield the (n, pn) reaction also.

(3) $n - p$ collisions with only the neutron emitted. This would yield a part of the (n, n') process. The final nucleus may boil off a proton to yield the $(n, n'p)$ or a neutron to give the $(n, n'n)$ reaction.

(4) $n - n$ collisions in which either or both of the neutrons are emitted. The latter would give rise to $(n, 2n)$ reaction while in the former case the residual nucleus can boil off either a proton or a neutron to yield the $(n, n'p)$ or the $(n, 2n)$ reaction respectively.

If we obtain the effective (n, n') spectrum due to (3) and (4) with one of the particles remaining inside the nucleus, then we can calculate the spectrum of protons due to $(n, n'p)$ reaction with the proton boiling off the residual nucleus as in the case of the compound process [*cf.* eq. (10)].

These various cross-sections are given by:

$$\left(\frac{d\sigma}{d\epsilon_p}\right)_{np} = \frac{\rho_p \left(\frac{d\sigma}{dx_2'}\right) \mathrm{T}(\epsilon_p)\, \phi(\epsilon_p)}{\epsilon_F{}^p \left[\rho_p a_{np} + \rho_n a_{nn} \frac{X_{nn}}{X_{np}}\right]} \tag{14}$$

$$\left(\frac{d\sigma}{d\epsilon_n}\right)_{np} = \frac{\rho_p \left(\frac{d\sigma}{dx_2''}\right) \mathrm{T}(\epsilon_n)\, \phi(\epsilon_n)\, [1 - \mathrm{T}(\epsilon_p)\, \phi(\epsilon_p)]}{\epsilon_F{}^p \left[\rho_p a_{np} + \rho_n a_{nn} \frac{X_{nn}}{X_{np}}\right]} \tag{15}$$

$$\left(\frac{d\sigma}{d\epsilon_n}\right)_{nn} = \frac{2\rho_n \left(\frac{d\sigma}{dx_2'''}\right) \mathrm{T}(\epsilon_n)\, \phi(\epsilon_n)\, [1 - \mathrm{T}(\epsilon_n')\, \phi(\epsilon_n')]}{\epsilon_F{}^n \left[\rho_p \frac{X_{np}}{X_{nn}} a_{np} + \rho_n a_{nn}\right]}. \tag{16}$$

T(E) is the penetrability and $\phi(\epsilon)$ takes into account loss due to attenuation in nuclear matter and due to reflection at the nuclear surface.

$$\phi(\epsilon) = \frac{e^{-0.75R/\lambda(\epsilon_0)}}{[1 - \{1 - \mathrm{T}(\epsilon)\}\, e^{-1.33R/\lambda(\epsilon_0)}]} \tag{17}$$

where $\lambda(\epsilon_0)$ is the mean free path of nucleons inside the nucleus with energy (E + V), V being the depth of the nuclear potential and E the energy of the nucleon outside the nuclear field.

$X_{np}(E_1)$ and $X_{nn}(E_1)$ are the total cross-sections for free $n - p$ and $n - n$ collisions with incident neutron energy E_1.

All other notations are the same as in ref. 10.

The functions $(d\sigma/dx_2')$, $(d\sigma/dx_2'')$, $(d\sigma/dx_2''')$ which occur in equations (14)–(16) are given by:

$$\left(\frac{d\sigma}{dx_2^{\nu}}\right) = \int_{x_2^{\nu}}^{1} \mathrm{F}(x_2, x_1)\, dx_2 \tag{18}$$

where x_2^{ν} is x_2', x_2'', or x_2''' are given by

$$\begin{aligned} x_2' &= 1 - (x_1 + Q' - x_p) \\ x_2'' &= 1 - (x_1 - x_n) \\ x_2''' &= 1 - (x_1' - x_n') \end{aligned} \tag{19}$$

where

$$x_1 = \frac{E_1 + V}{\epsilon_F{}^p}; \qquad Q' = \frac{Q}{\epsilon_F{}^p}; \qquad x_p = \frac{E_p + V}{\epsilon_F{}^p}$$

$$x_n = \frac{E_n + V}{\epsilon_F{}^p}; \qquad x_n{}' = \frac{E_n + V}{\epsilon_F{}^n}; \qquad x_1{}' = \frac{E_1 + V}{\epsilon_F{}^n}$$

$$\epsilon_F{}^p = V - B_p; \qquad \epsilon_F{}^n = V - B_n. \tag{20}$$

B_n and B_p are the binding energies of the last neutron and proton in the nucleus respectively.

$$F(x_2, x_1) = \frac{3}{4} \frac{1}{\sqrt{2(x_1 + x_2)}} \tanh^{-1} \left(\frac{2x_2{}^{\frac{1}{2}} \sqrt{2(x_1 + x_2)}}{x_1 + 3x_2} \right) \tag{21}$$

In (21), x_1 is to be replaced by x_1' for the case $x_2 = x_2'''$. Figure 1 gives values of $(d\sigma/dx_2{}^p)$ for various values of x_1 as a function of x_2.

We can define a general function $\alpha(x_3)$ given by

$$\alpha(x_3) = \int_{x_2{}^p}^{1} \left(\frac{d\sigma}{dx_2{}^p} \right) dx_2{}^p \tag{22}$$

where, $x_3 = 2 - (x_1 + Q')$ for (n, p) and $(2x - x_1')$ for (n, n'). From equation (22) α_{nn} and α_{np} can be evaluated. Figure 2 gives $\alpha(x_3)$ as a function of x_3

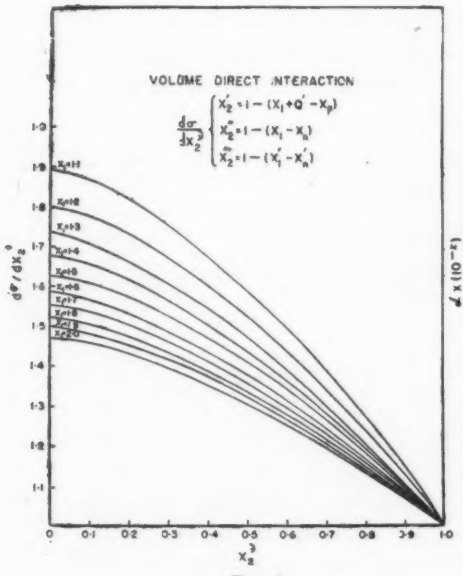

FIG. 1

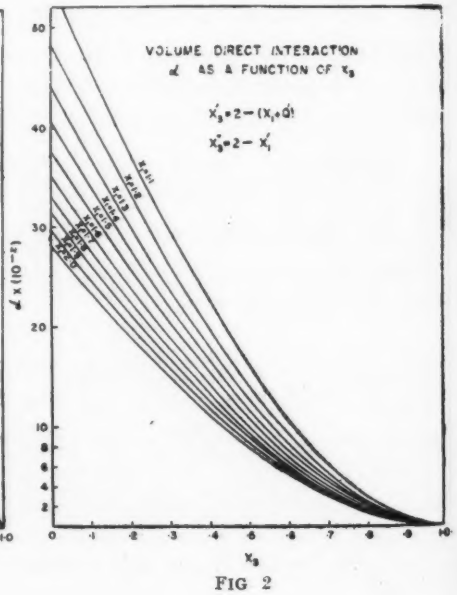

FIG 2

for various values of x_1. From these two figures the various direct interaction cross-sections can be evaluated for any nucleus.

Neutron and Proton Penetrabilities.—The cross-section $\sigma_c(\epsilon)$ for the formation of the compound nucleus due to an incident particle of energy E with a target nucleus is given by

$$\sigma_c(E) = \pi\lambda\!\!\!^{-2} \sum_l (2l+1)\, T_l(E) \tag{23}$$

where $T_l(E)$ are the partial penetrabilities as defined by Blatt and Weisskopf.[16] The penetrabilities T(E) which occur in the above derivation for the proton spectra are defined as

$$T(E) = \frac{\sigma_c(E)}{[\pi(R+\lambda\!\!\!^{-})^2]} \tag{24}$$

where $\lambda\!\!\!^{-} = (\lambda/2\pi)$, λ being the wavelength of the incident particle and R is the incident channel radius. We have chosen for R the value of $1{\cdot}5\,A^{1/3}$ Fermis.

For square well potential for protons $\sigma_c(E)$ has been calculated from the computations of $T_l(E)$ by Feshbach *et al.*[18]

The penetrabilities for charged particles have been calculated by Kikuchi[11] using the W.K.B. approximation. We have chosen the same potential for evaluating T(E). The potential is given by

$$V(r) = V_c(r) + V_n(r)$$

$$V_c(r) = \frac{ZZ'e^2}{r}$$

$$V_n(r) = -V\left(\frac{1+\exp.(r-a)}{b}\right)^{-1} \tag{25}$$

where $V_c(r)$ and $V_n(r)$ are the Coulomb and nuclear potentials respectively. We have chosen for the constants the values: $a = 4{\cdot}1\,f$; $b = 0{\cdot}5\,f$. Then T(E) is given in the W.K.B. approximation by

$$T(E) = \exp.\left[-2\sqrt{\frac{2M}{\hbar^2}}\int_{r_1}^{r_2}\sqrt{V(r)-E}\,dr\right] \tag{26}$$

where r_1 and r_2 are obtained from the zeros of the function $[V(r) - E]$. Since the above approximation does not take into account the centrifugal force, it would yield a much higher value for the penetrability of high energy protons than given by the exact solution. To some extent this has been corrected for by smooth extrapolation of the above curve for low energy protons with the asymptotic value of T(E) given by

$$[T(E)]_{asymp.} = \left[1 - \frac{R}{(R + \lambda)\frac{E}{B}}\right] \tag{27}$$

where B is the Coulomb barrier height for the nucleus. Figure 3 gives the penetrability as a function of proton energy for Mg^{27} for square and diffuse potentials.

Results and Discussion

The above theory has been applied to compute the energy spectra of protons emitted from Al^{27} nucleus due to neutron interaction. The incident neutron energies chosen are 14·7 MeV and 17·5 MeV. The constants used in the computation are given in Table I. The value of 'a' which occurs in the level density formula has been varied from 1·5 MeV^{-1} to 3 MeV^{-1} in steps of 0·5 MeV^{-1}.

Figure 4 gives a typical spectrum computed for an incident energy of 14·7 MeV together with contributions from the various types of reactions considered above. It is seen from the figure that the contribution due to direct interaction is negligibly small and does not alter the shape of the total spectra appreciably except in the very high energy part. Since the differential cross-section for high energy proton emission is small, experimental data have large statistical errors and hence cannot resolve the effect due to

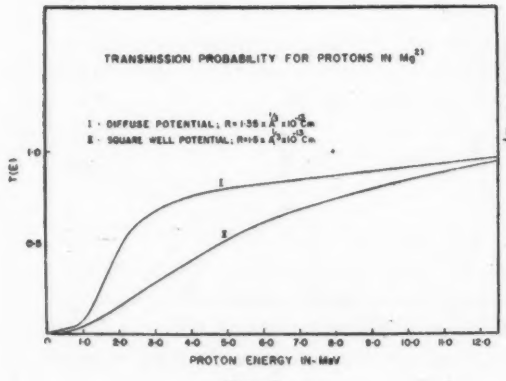

FIG. 3

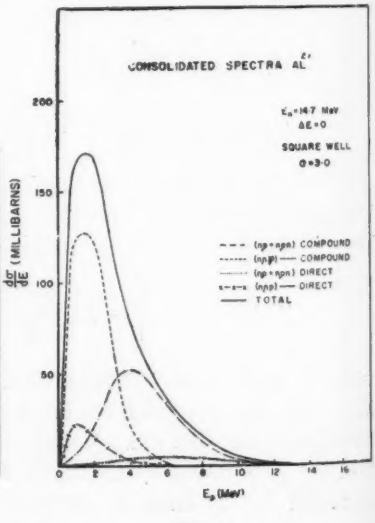

FIG. 4

direct interactions. The only other method of evaluating the direct interaction cross-section from experimental data is to study the angular distribution. Allen[1] uses this procedure and assumes that the total non-isotropic part of the distribution is due to direct interaction. It has been shown by Ericson and Strutinski[4] that the angular distribution in the statistical model need not be isotropic and a more realistic assumption would be that it is of the form $(A + B\cos^2\theta)$. The experimental angular distributions are not accurate enough to permit such an analysis.

Figures 5–8 give $\log_e \omega(E)$ as a function of E, for the two types of potentials and level density formulae that we have used. Here $\omega(E)$ and E are defined as:

$$\omega(E) = \frac{N(\epsilon_p)\, d\epsilon_p}{\epsilon_p\, [\sigma_c(\epsilon_p)]_{\text{square well}}} \tag{28}$$

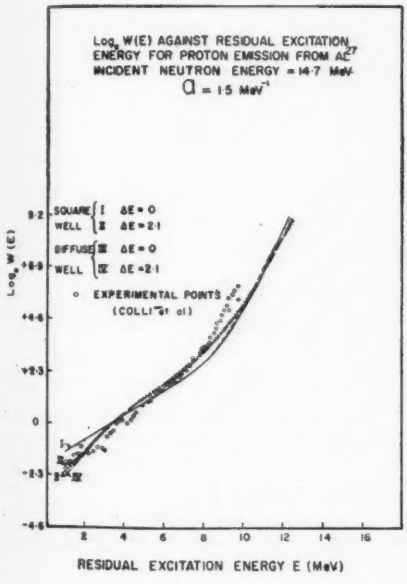
Log$_e$ W(E) AGAINST RESIDUAL EXCITATION ENERGY FOR PROTON EMISSION FROM Al^{27}
INCIDENT NEUTRON ENERGY = 14·7 MeV
a = 1·5 MeV^{-1}
SQUARE WELL I ΔE = 0
II ΔE = 2·1
DIFFUSE WELL III ΔE = 0
IV ΔE = 2·1
o EXPERIMENTAL POINTS (COLLI et al)
Log$_e$ W(E)
RESIDUAL EXCITATION ENERGY E (MeV)

FIG. 5

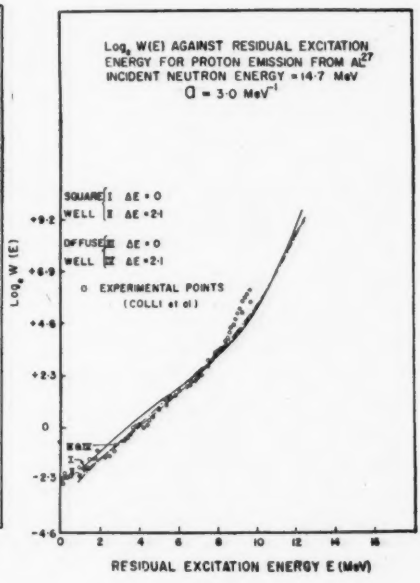
Log$_e$ W(E) AGAINST RESIDUAL EXCITATION ENERGY FOR PROTON EMISSION FROM Al^{27}
INCIDENT NEUTRON ENERGY = 14·7 MeV
a = 3·0 MeV^{-1}
SQUARE WELL I ΔE = 0
II ΔE = 2·1
DIFFUSE WELL III ΔE = 0
IV ΔE = 2·1
o EXPERIMENTAL POINTS (COLLI et al)
Log$_e$ W(E)
RESIDUAL EXCITATION ENERGY E (MeV)

FIG. 6

and $E = E_{np}^{0} - \epsilon_p$ where E is the residual excitation energy if all the protons were emitted through the (n, p) and (n, pn) reactions only. E_{np}^{0} is the maximum proton energy possible for these reactions and ϵ_p is the energy of the emitted proton. $N(\epsilon_p)\, d\epsilon_p$ is the spectrum of protons emitted due to all the various types of reactions considered above. The reason for this

TABLE I

Binding energy[20] of protons in:

Al^{28} ..... 9·5 MeV.

Al^{27} ..... 8·3 MeV.

of neutrons in:

Al^{28} ..... 7·7 MeV.

Al^{27} ..... 13·0 MeV.

Mg^{27} ..... 6·4 MeV.

Cross-sections	14·7 MeV.	17·5 MeV.
$\sigma\,(n, p)^{15}$	53 mb.*	38 mb.*
$\sigma\,(n, \alpha)^{15}$	120 mb.	80 mb.
σ_{ss}[22]	960 mb.	900 mb.
σ_I	860 mb.	830 mb.†

Paring Energy[17]

Mg^{26} .....2·1 MeV

Mg^{27} .....4·3 MeV

Al^{27} .....2·2 MeV

V = Nuclear potential = 42 MeV‡

* This value corresponds to 60 mb. at 14 MeV and is lower than the one used in reference 15. This lower value seems to agree better with experiment and is the value obtained by Paul and Clarke[21] and by Allen.[1]

† The σ_I has been calculated from the formula $\sigma_I = \pi(R + \lambda)^2$.

‡ This is the value obtained from the real part of the optical potential and seems to fit the total as well as the elastic neutron cross-section. Proton scattering data also yield a similar value.

choice of definition is because the experimental data of Colli *et al.*[5] is also represented in the same way. It is seen from Figs. 5–8 that the experimental points agree better for the case $a = 3\ \text{MeV}^{-1}$ than for $a = 1{\cdot}5\ \text{MeV}^{-1}$. The function $\log_e \omega\,(E)$ is very insensitive to the type of potential used or to the level density formula assumed. The experimental points seem to be in better agreement with the square well potential for $\Delta E = 2{\cdot}1$ MeV

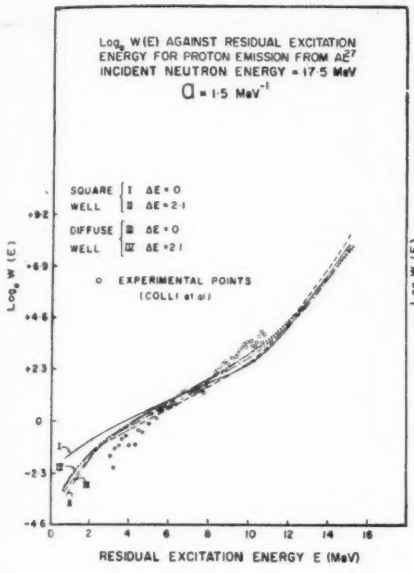
Log$_{10}$ W(E) AGAINST RESIDUAL EXCITATION ENERGY FOR PROTON EMISSION FROM Al^{27}
INCIDENT NEUTRON ENERGY = 17·5 MeV
a = 1·5 MeV^{-1}
SQUARE WELL I ΔE = 0
II ΔE = 2·1
DIFFUSE WELL III ΔE = 0
IV ΔE = 2·1
o EXPERIMENTAL POINTS (COLLI et al)
Log$_{10}$ W (E)
RESIDUAL EXCITATION ENERGY E (MeV)

FIG. 7

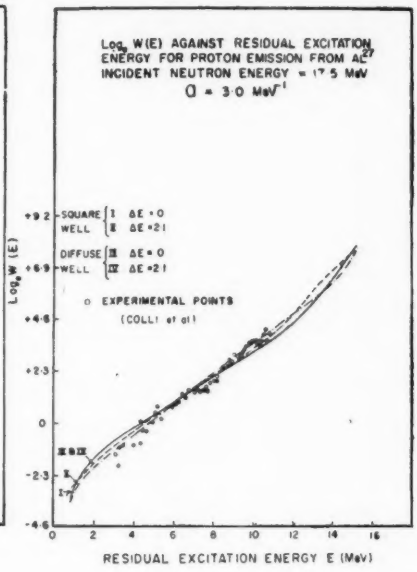
Log$_{10}$ W(E) AGAINST RESIDUAL EXCITATION ENERGY FOR PROTON EMISSION FROM Al^{27}
INCIDENT NEUTRON ENERGY = 17·5 MeV
a = 3·0 MeV^{-1}
SQUARE WELL I ΔE = 0
II ΔE = 2·1
DIFFUSE WELL III ΔE = 0
IV ΔE = 2·1
o EXPERIMENTAL POINTS (COLLI et al)
Log$_{10}$ W (E)
RESIDUAL EXCITATION ENERGY E (MeV)

FIG. 8

but no definite conclusion can be reached since the experimental errors are fairly large. The discrepancy between the 14·7 MeV data as pointed out by Colli *et al.*[5] is only due to the (n, np) reaction.

The total cross-section for the proton production is more sensitive to the potential used and to the level density formula. Unfortunately we are unable to compare our results with the experimental data because of the large error introduced in the computation of the (n, n') cross-section from the total non-elastic cross-section. This can be avoided by a direct measurement of the (n, n') cross-section. There seems to be some discrepancy in the total cross-sections for the various reactions but unless more accurate cross-section measurements are available nothing more conclusive can be derived from the present data. The deviation of the experimental data from the theoretical curves in Figs. 5–8 for large value of E may be due to errors in our estimation of the (n, n') cross-section and our assumption of constant 'a' for all these nuclei.

The experimental data for the differential cross-section for direct interaction obtained by Allen[1] from angular distribution is compared with the theory in Figs. 9 and 10. The experimental points have been evaluated on the assumption that the statistical model yields isotropic angular

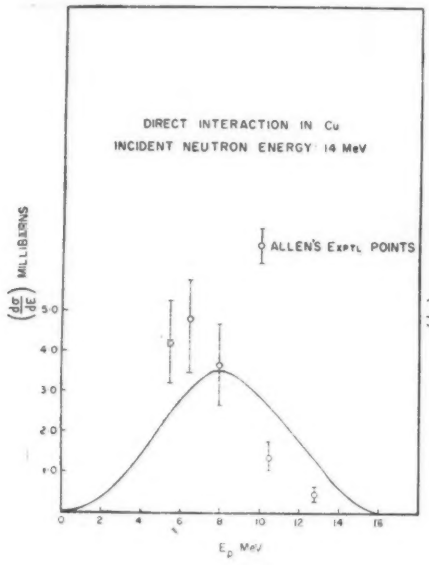

FIG. 9

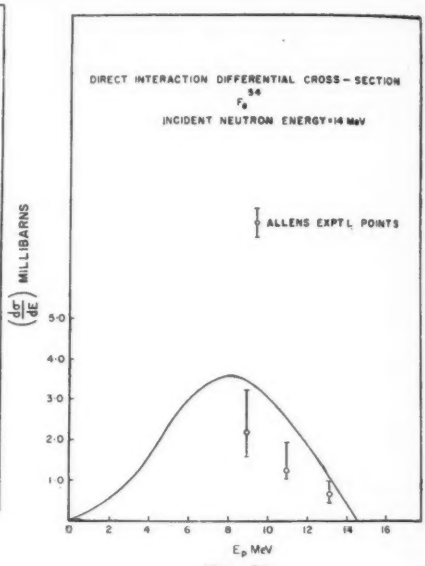

FIG. 10

distribution. Since the data have large experimental errors, it is not possible to analyse it in terms of the $A + B\cos^2\theta$ distribution. In the theoretical curve we have used the value of 0·25 for X_{nn}/X_{np}, the ratio of free $n-n$ to $n-p$ cross-section. The actual value for this ratio lies between 0·25 and 0·50[19] and a higher value for this ratio would give a better fit to the experimental data. It seems from these figures that at least for nuclei in this region the major contribution to direct interaction is from volume effects.

The above analysis indicates that a combined measurement of the various cross-sections as well as the energy and angular distribution of the emitted protons is needed for detailed analysis of these reactions. Also the present data are not accurate enough to decide between the types of potential or level density formula.

We should like to thank Dr. A. M. Lane, Dr. T. Ericson and Dr. E. B. Paul for reading the manuscript and supplying us with valuable comments.

We gratefully acknowledge the valuable help of Shri M. R. Hiranandani in the above computations.

References

1. Allen, D. L. .. *Proc. Phys. Soc.*, 1957, **70 A,** 195; *Nuclear Phys.*, 1959, **10,** 348.
2. Gugelot, P. C. .. *Phys. Rev.*, 1954, **93,** 425.
3. Badoni, C., Colli, L. and Facchini, U. *Nuvo Cimento*, 1956, **4,** 1618.
   Colli, L. and Facchini, U. *Ibid.*, 1957, **5,** 309.
   ———— and Micheletti, S. *Ibid.*, 1957, **5,** 502.
4. Wolfenstein, L. .. *Physics Rev.*, 1951, **82,** 690.
   Ericson, T. and Strutinski, V. *Nuclear Phys.*, 1958, **8,** 284.
5. Colli, L., Pignanelli, M., Rytz, A. and Zurmuhle, R. *Nuvo Cimento*, 1958, **9,** 280.
6. Austern, N., Butler, S. T. and MacManus, H. *Phys. Rev.*, 1953, **92,** 350.
7. Clementel, E. and Villi, C. *Nuvo Cimento*, 1958, **9,** 950.
8. Goldberger, M. L. .. *Phys. Rev.*, 1948, **74,** 1269.
9. Hayakawa, S., Kawai, M. and Kikuchi, K. *Prog. of Theor. Phys.*, 1955, **13,** 415.
10. Brown, G. and Muirhead, H. .. *Phil. Mag.*, 1957, **2,** 473.
11. Kikuchi, K. .. *Prog. of Theor. Phys.*, 1957, **17,** 643.
12. Newton, T. D. .. *Can. J. Phys.*, 1956, **34,** 804.
13. Elton, L. R. B. and Gomes, L. C. *Phys. Rev.*, 1957, **105,** 1027.
14. Lane, A. M. and Wandal, C. F. *Ibid.*, 1955, **98,** 1524.
15. Mani, G. S., McCallum, G. J. and Fergusson, A. T. G. *Nuclear Physics* (to be published).
16. Blatt, J. M. and Weisskopf, V. F. *Theoretical Nuclear Physics*, John Wiley and Sons, 1952.
17. Cameron, A. G. W. *Can. J. Phys.*, 1957, **35,** 1021; 1958, **36,** 1040.
18. Feshbach, H., Shapiro, M. M. and Weisskopf, V. F. *Tables for the Penetrabilities of Charged Particles*, NYO 3077 (1953).
19. Hess, W. N. .. *Rev. Mod. Phys.*, 1958, **30,** 368.
20. Wapstra, A. H. .. *Physica*, 1955, **21,** 367.
21. Paul, E. B. and Clarke, R. L. *Can. J. Phys.*, 1953, **31,** 267.
22. Hughes, D. J. and Schwartz, B. *Neutron Cross-sections*, BNL 325 (1958).

THERMAL DIFFUSIVITY OF A ROOF SLAB FROM *IN SITU* TEMPERATURE MEASUREMENTS

By B. C. Raychaudhuri

(*Central Building Research Institute, Roorkee*)

Received September 24, 1959

(Communicated by T. N. Seshadri, F.A.SC.)

Introduction

The flow of heat through a roof slab is periodic, on account of the solar insolation, which imposes a diurnal variation of temperature on its exposed surface. The exact periodicity can be vitiated by the small difference that may occur between the initial and final temperatures for the 24-hour interval: but this difference is usually negligible, especially when the day forms part of a stable synoptic regime. The significant thermal property of the roof material is not so much its thermal conductivity (K), as its thermal diffusivity, α given by the relation

$$\alpha = \frac{K}{\rho C_p}$$

where ρ and C_p are its density and specific heat respectively.

In common practice, α is calculated from the experimental values of K, ρ, and C_p measured under steady state conditions for oven-dry specimens. The temperature dependence of these constants may be a second order effect only; but it is definitely known that they vary with the moisture content of the material. Since the air in the pores of a moist specimen is replaced by the more conducting water both in its liquid and vapour phases, not only the effective ρ, and C_p but K also alters. A vapour pressure gradient is set up due to temperature differences; and the consequent vapour movement inside gives rise to an additional heat transport, both latent and sensible, in parallel to the conduction flow. This reduces the thermal resistance or increases the apparent conductivity of the material.

Considerable errors are therefore likely to be introduced in the analysis of heat transfer through building sections if α is calculated from the conventionally determined values of K, ρ and C_p. The correct approach would be to evolve a method of determining α of the material directly under the existing conditions of moisture.

An attempt is made in this paper to obtain a value for α for a roof slab from *in situ* temperature measurements of its outside and inside surfaces and of the ambient air inside the room below.

Experimental

Temperature data were available already, for the living rooms of about 40 dwelling houses put up for the Low Cost Housing Exhibition at Delhi (Raychaudhuri, 1957). Thermocouples were set up at a number of points in the experimental rooms and hourly temperatures were recorded continuously for a number of days, to an accuracy of $\pm 0{\cdot}1°$ F.

The data used in this paper were that obtained for one of the rooms, kept completely closed throughout a clear day (22nd April 1955) in the middle of a stable stretch of weather conditions. The roof of the room was a $4\frac{1}{2}''$ R.C.C. slab. The room was $10'\ 6'' \times 12' \times 9'\ 9''$ in dimensions and built with 9″ brick walls in cement mortar, plastered on both sides.

Curves for the observed surface temperatures of the roof (outside) the ceiling (inside) and the ambient air temperature at the centre of the room, on the chosen day are given in Fig. 1.

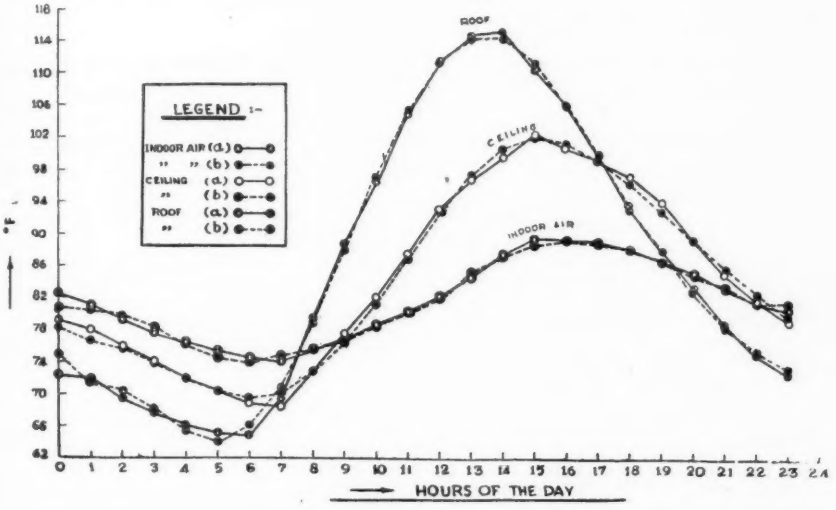

Fig. 1. Time-temperature curves for roof ceiling and indoor ambient air, (*a*) As observed, (*b*) As synthesised from the Fourier components.

THEORETICAL

Houghten (1932) and his co-workers have given a solution for the ceiling temperature, θ_c consequent on a unidirectional transverse flow of heat from the roof surface where the temperature varies sinusodially, with an amplitude θ_1.

The solution is given below in a slightly altered form

$$\theta_c = R_1 e^{-\beta_1 l}\theta_1 \sin(\omega t - \beta_1 l + \gamma_1) \tag{1}$$

where l is the thickness of the roof slab;

$$\beta_1 = \sqrt{\frac{\omega}{2\alpha}}, \quad \left(\omega = \frac{2\pi}{T} = 15°/\text{hr.}\right)$$

$$R_1 = \frac{2\sqrt{2}}{\sqrt{2 + 2f_1 + f_1^2}};$$

$$\gamma_1 = \tan^{-1}\frac{f_1}{2 + f_1};$$

$$f_1 = \frac{h}{K\beta_1},$$

and h is the appropriate film transfer coefficient, equal to the ratio between the rate of heat transfer per unit area of the ceiling and the ceiling-to-air difference in temperature.

h, K and the ambient air temperature for the room below are assumed constant throughout the period while arriving at the above solution.

This solution can be extended to the case where the roof temperature has any periodic variation other than simple sinusodial. θ_c will now be given by the expression

$$\theta_c = \bar{\theta}_c + \sum_{n=1}^{\infty} R_n e^{-\beta_n l}\theta_n \cos(n\omega t - \sigma_n - \beta_n l + \gamma_n) \tag{2}$$

when the roof temperature is given by the Fourier expansion

$$\theta_r = \bar{\theta}_r + \sum_{n=1}^{\infty} \theta_n \cos(n\omega t - \sigma_n)$$

where

$$\beta_n = \sqrt{n}\beta_1;$$

$$R_n = \frac{2\sqrt{2}}{\sqrt{2 + 2f_n + f_n^2}};$$

$$\gamma_n = \tan^{-1} \frac{f_n}{2 + f_n}$$

and

$$f_n = \frac{f_1}{\sqrt{n}}.$$

$\overline{\theta}_r$ and $\overline{\theta}_c$ are related to $\overline{\theta}_a$, the assumed constant air temperature by the steady state equation

$$\frac{K}{l}(\overline{\theta}_r - \overline{\theta}_c) = h(\overline{\theta}_c - \overline{\theta}_a)$$

$$\frac{h}{K} = \frac{(\overline{\theta}_r - \overline{\theta}_c)}{(\overline{\theta}_c - \overline{\theta}_a)} \times \frac{1}{l}. \tag{3}$$

Procedure

The observed experimental time temperature curves of the roof (θ_r), the ceiling (θ_c) and the indoor ambient air (θ_a) are first analysed into their Fourier components as follows:

$$\begin{aligned}\theta_r = 86{\cdot}07 &+ 23{\cdot}02 \cos(\omega t - 214^\circ 9') \\ &+ 6{\cdot}85 \cos(2\omega t - 27^\circ 59') \\ &+ 1{\cdot}01 \cos(3\omega t - 115^\circ 50') \\ &+ 0{\cdot}50 \cos(4\omega t - 130^\circ 22') \\ &+ \ldots\ldots\end{aligned} \tag{4}$$

$$\begin{aligned}\theta_c = 84{\cdot}33 &+ 14{\cdot}95 \cos(\omega t - 242^\circ 35') \\ &+ 3{\cdot}66 \cos(2\omega t - 70^\circ 30') \\ &+ 0{\cdot}32 \cos(3\omega t - 163^\circ 50') \\ &+ 0{\cdot}25 \cos(4\omega t - 139^\circ 31') \\ &+ \ldots\ldots\end{aligned} \tag{5}$$

$$\begin{aligned}\theta_a = 81{\cdot}45 &+ 6{\cdot}50 \cos(\omega t - 259^\circ 54') \\ &+ 1{\cdot}76 \cos(2\omega t - 84^\circ 48') \\ &+ 0{\cdot}71 \cos(3\omega t - 56^\circ 44') \\ &+ 0{\cdot}34 \cos(4\omega t - 117^\circ 17') \\ &+ \ldots\ldots\end{aligned} \tag{6}$$

The curves, summing up the first five terms of the Fourier expansions for θ_r, θ_c and θ_a, are also given in Fig. 1 along with the observed curves. The correspondence between the two justifies limiting the calculations to the fundamental and the first three harmonics only and neglecting as insignificant the succeeding terms of the Fourier series.

It is to be noticed that the ambient air-temperature is not constant as assumed in the solution (Equation 2). However, if it is taken as constant at its mean value, $\overline{\theta}_a$ during the entire period, the solution for the ceiling temperature (Equation 2) can be applied as a first approximation, and more so when $\theta_a = \overline{\theta}_a = 81{\cdot}45°$ F., at the instant defined by $\omega t = 175°\ 16'$ (as obtained from Equation 6).

The next step would be to solve for α. But due to the inherent difficulty in employing the solution directly, an indirect method is adopted. The values of θ_c, the ceiling temperatures are computed at the instant corresponding to $\omega t = 175°\ 16'$, for different values of α from Equation 2, and substituting for h/K the value 1·609 as calculated from Equation 3. The relationship between α and the computed values of θ_c at the specified instant ($\omega t = 175°\ 16'$) is shown graphically in Fig. 2. The observed value of θ_c at the instant is 90·82

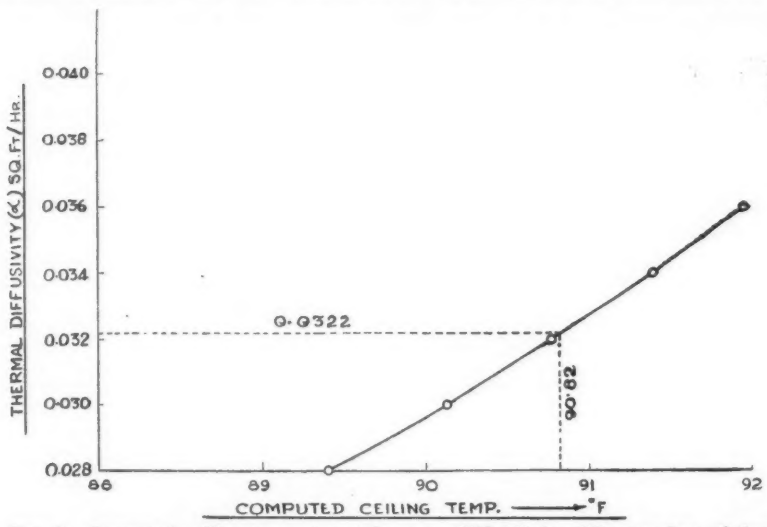

FIG. 2. Computed ceiling temperature (when wt. = 175° 16′) for different values of thermal diffusivity.

(as obtained from Equation 5), which when interpolated in the curve of Fig. 2 gives the value for α as 0·0322 sq.ft. per hour.

The ceiling temperature for the full cycle computed for this value of α can now be expressed by the equation:

$$\begin{aligned}\theta_c = 84{\cdot}33 &+ 14{\cdot}86 \cos(\omega t - 241^\circ 33') \\ &+ 3{\cdot}59 \cos(2\omega t - 76^\circ 50') \\ &+ 0{\cdot}44 \cos(3\omega t - 180^\circ 15') \\ &+ 0{\cdot}18 \cos(4\omega t - 207^\circ 34') \end{aligned} \quad (7)$$

The curve of Equation 7 is given in Fig. 3, along with the experimental curve for the ceiling as defined by Equation 5. The correspondence between the two curves is good and the two coincide as they should when $\theta_a = \overline{\theta}_a$. The discrepancy, where it exists, should be ascribed to the fact that the air temperature was not constant throughout as was assumed. Also the value of h can vary with time, being greater during the later hours of the night and early morning on account of a convective regime set up in the room air, θ_c being less than θ_a then (*vide* Fig. 3, where the room air temperature curve is also given for easy reference). During the rest of the period a stratified regime is set up as $\theta_c > \theta_a$ at that time. The reflections on the ceiling temperatures due to variations in θ_a and h will be greater during nights but in opposing directions. This will displace the observed curve above the calculated curve at first with a possibility of the two crossing over and the former coming below the latter after some time. During the day and up to about midnight the observed curve will be throughout above the calculated curve, as the effects due to h and θ_a are additive then: but the shift may now be smaller in magnitude than that during nights as the relative variations in h and θ_a from their average values are less during this period. These inferences, necessarily qualitative, are borne out by Fig. 3.

To a first degree of approximation at least, the value of α for the roof can be taken as 0·032 sq.ft./hr. based on *in situ* temperature measurements and the method of calculation adopted. This value of α is the average value of the thermal diffusivity of the roof slab for the complete cycle of 24 hours under existing conditions of moisture.

Summary and Conclusion

An attempt is made in this paper to compute the value of α for the roof material from *in situ* temperature measurements of roof and ceiling surfaces and indoor ambient air below, using the Fourier Components of the periodic variations and the available classical methods of solution for the general differential equation of unidirectional heat flow through the structure. Even

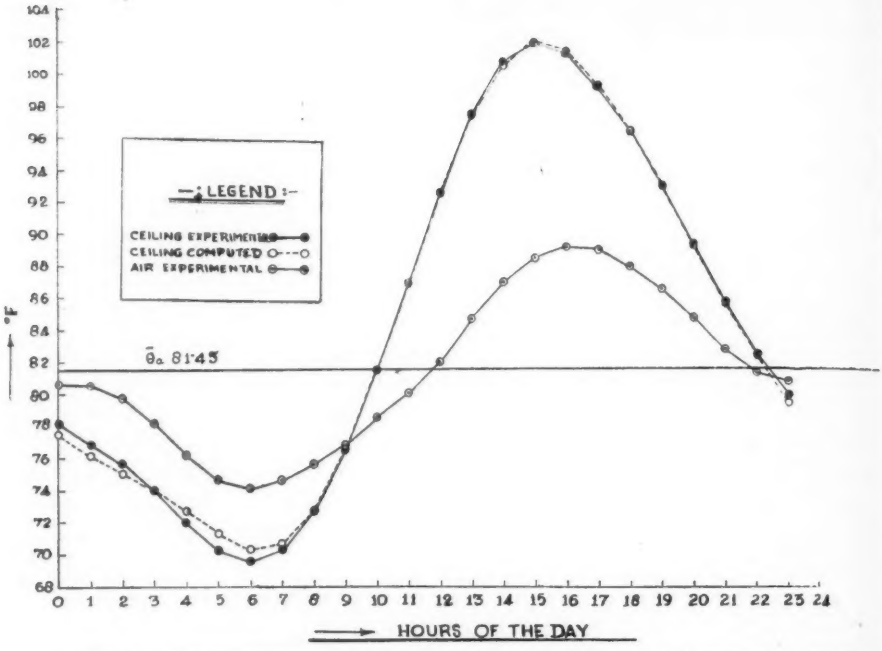

FIG. 3. Time-temperature curves for the ceiling, experimental and computed (Experimental air temperature curve is also given).

though the boundary conditions assumed in the solution are not strictly identical with the experimental ones the computed thermal diffusivity, under *in situ* conditions, can be considered accurate enough for practical purposes.

ACKNOWLEDGEMENTS

Thanks are due to Prof. T. N. Seshadri, Asst. Director, for his sustained interest in this work and his valuable help by way of useful discussions and suggestions, to Shri D. P. Garg for his assistance in the numerical computations and to the Director, Central Building Research Institute, for his kind permission to publish this paper.

REFERENCES

1. Houghton, F. C., Blackshaw, J. L., Pugh, E. M. and McDermott, P. — *Trans. Am. Soc. Heat. Vent. Eng.*, 1932, **38**, 260.

2. Raychaudhuri, B. C. .. *Report on Low Cost Housing*, Government of India, New Delhi, January 1957, p. 61.

A SIMPLE METHOD FOR MEASURING POROSITY IN ROCKS

By S. Balakrishna and G. Shankar Narayana

(Geology Department, Osmania University, Hyderabad-7)

Received March 24, 1960

(Communicated by Dr. S. Bhagavantam, F.A.SC.)

1. Introduction

The measurement of porosity of a rock involves the evaluation of its pore volume and bulk volume. Any method that will enable the reliable determination of these quantities may be employed. The bulk volume can be determined either by direct measurement of its geometric form or by displacement of an equivalent volume of suitable liquid by immersing the coated specimen. The measurement of pore volume is an important and difficult feature of this experiment and several methods have been employed for this purpose. Tickell and others (1933) devised a porosimeter employing the phenomenon of change of length of mercury column with volume change in a manometer. Fancher (1950) employed the familiar Russel volumeter to measure the porosity of consolidated samples by saturating the sample with a suitable fluid and then observing the displacement or loss of weight resulting from immersion. Hughes and Cooke (1953) measured the porosity of rocks by using a modified Boyles Law apparatus which involves the evacuation of air contained in a rock by a pump. Davis (1954) suggested an empirical formula for estimating the porosity of sedimentary rocks from the bulk density. He had also shown that such estimated values closely agree with (3% discrepancy) the experimental results. The authors in the present investigation have employed Tickell's porosimeter with certain important modifications which make the method simpler and the results repeatable. The ease and accuracy with which the pore volume could be determined for a given rock and thereby the porosity calculated from its bulk volume is the essential feature of this method.

2. Experimental Technique

Figure 1 shows the modified form of Tickell's porosimeter. The chief modifications introduced are:

(1) The height of the specimen chamber is increased to handle bigger samples.

(2) The constancy of the mercury level at the bottom is maintained by keeping a small dish in another bigger dish and thereby allowing for an overflow, instead of a shallow dish employed by Tickell, where the level of mercury is not likely to be constant.

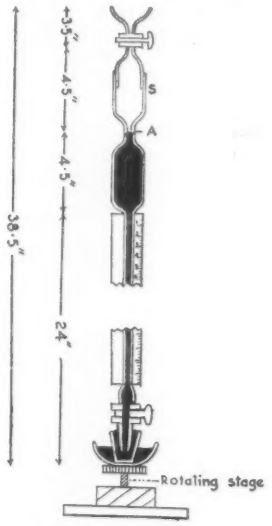

FIG. 1. Porosimeter.

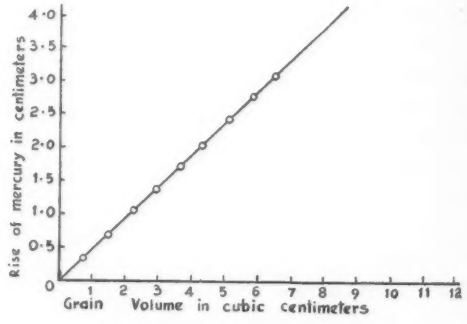

FIG. 2. Calibration Graph.

The bulk volume of the specimen is determined by measuring its geometric dimensions. Closing the lower stop-cock, mercury is poured in the vertical tube to the mark (A). By closing the upper stop-cock and releasing the lower stop-cock, mercury is allowed to fall into the dish and attain a steady state which is taken as initial reading (I_1). Again mercury is refilled to the mark (A) and in fact this operation is to be done whenever a fresh reading is to be taken. The dry specimen whose bulk volume is already determined is introduced in the specimen chamber (S). By releasing lower stop-cock, mercury is now allowed to come to rest at a higher position (I_2), since there is a reduction of air in (S) due to the grain volume of the sample. The difference between I_2 and I_1 will be the length of mercury column corresponding to the grain volume itself. Care has been taken to see that joints are airtight and the instrument is free from air-bubbles. From a knowledge of I_2–I_1, the grain volume is then read off from an already prepared calibration graph (Fig. 2). From the knowledge of the bulk volume and grain volume, the pore volume is calculated from which the effective porosity (P%) is computed.

The instrument is calibrated by taking a number of uniform ball-bearing shots (0·723 c.c.). As these B.B. shots are assumed to be practically non-porous, the rise in mercury column is due to the displacement of equivalent volume of air as a result of insertion of specimens in the chamber (S). Figure 2 shows the graph connecting the volume of ball-bearing shots with the corresponding rise in mercury level (I_2–I_1) for the apparatus we have constructed. It can be seen from the graph that every 1 c.c. increase of volume will result in rise of mercury column to 0·5 cm. approximately. Further, the variation is found to be strictly linear as should be expected.

The rock specimens chosen here are of definite geometric shape usually of rectangular parallelepipeds. Such specimens will enable us to determine the bulk volume easily without taking recourse tc wax coating and subsequent measurement by displacing a suitable liquid equivalent to its volume as done by other workers. The present method enables us to repeat our experiments and get the mean values while in other methods this becomes an impossibility. Another significant feature is that the specimen does not come into contact with the liquid. Air, because of its nearly perfect expansibility and low viscosity, penetrates the small and poorly connected pore spaces and gives a more accurate measurement of the effective porosity. This method is not affected by the variation of atmospheric pressure as we are taking I_1 and I_2, at the same time and temperature correction is made whenever required.

3. Results and Discussion

Employing the porosimeter described above and taking all possible precautions, measurements have been made in some limestones and sandstones. Results are given in Table I. Here density (ρ) is in grams/c.c., surface area (S.A.) is in square cm., Bulk Volume (B) is in cubic cm., difference in mercury level I_2–I_1 is in cm., grain volume (G) is in cubic cm. as read off from the calibration graph. Porosity (P%) is given as a percentage.

I_1 is 21·2 at room temperature 27° C. and atmospheric pressure 760 mm.

The values (Table I) are mean values of readings obtained a number of times. The values are repeatable and the accuracy is found to be fairly high.

The empirical formula suggested by Davis and referred to earlier for estimating the porosity (ϕ) in sedimentary rocks from Bulk density (ρ_b) in C.G.S. Units is

$$\phi = \left[\frac{2{\cdot}654 - \rho_b}{1{\cdot}654}\right] \times 100.$$

TABLE I

Porosity values

Specimen	ρ	S.A. sq.cm.	B c.c.	I_1-I_2 cm.	G c.c.	P%
Limestone—						
1 ..	2·7	8·98	1·818	0·8	1·7	6·49
2 ..	2·7	13·144	3·027	1·4	2·95	5·15
3 ..	2·7	35·897	10·85	5·1	10·65	1·84
4 ..	2·7	38·918	11·48	5·4	11·3	1·57
Sandstone—						
1 ..	2·47	24·138	5·615	2·1	4·3	23·44
2 ..	2·47	30·09	7·413	2·8	5·8	22·4
3 ..	2·47	34·687	9·05	3·4	7·1	21·55
4 ..	2·47	45·425	12·72	4·9	10·25	19·42

The expected or mean error in ϕ was shown by him to be small and equal to about 3%. The authors have calculated the porosity employing this formula and the results (*a*) are tabulated in Table II along with the porosity values measured by the conventional method (*b*). Mean values obtained in the present investigation (*c*) are given for comparison.

TABLE II

Comparison of porosity values

Specimen	*a*	*b*	*c*
Limestone ..	2·05	1·96	1·84
Sandstone ..	20·19	19·20	19·42

The results in Table II are in good agreement with each other.

In order to study the effect of size and surface area, number of parallelepipeds of limestones and sandstones have been prepared (perfect rectangular shape) and the results obtained are given in Table I.

Figure 3 shows the change in porosity value with surface area of the specimen. The graph shows that the porosity approaches constancy with increase in surface area in relation to bulk volume. Thus it can be seen that best results can be obtained by taking a number of small samples to

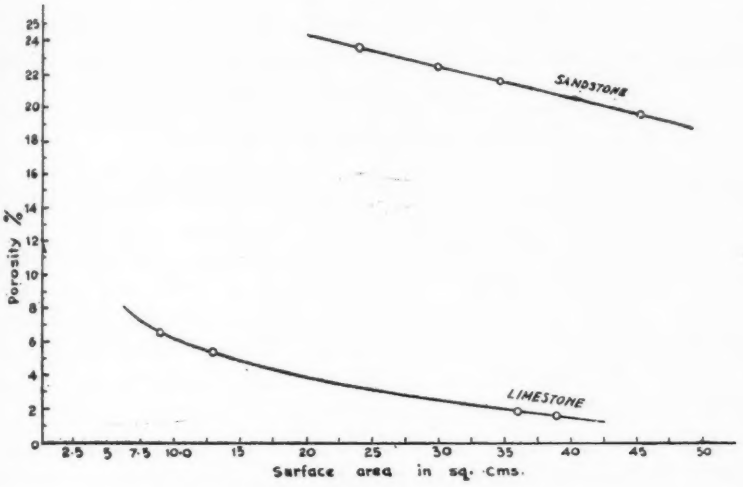

FIG. 3. Variation of Porosity with Surface Area.

fill up the chamber rather than by taking one big sample. This is what one should expect. Care should be taken to see that the sample surfaces are plane parallel in order to get good results.

4. CONCLUSION

A simple porosimeter has been designed with a view to handle large volumes of samples and determine the grain volume with the help of a calibration graph. Bulk volume is determined directly from the geometric shape of the samples. The results obtained are repeatable and are found to be in good agreement with those obtained by other methods.

REFERENCES

Davis, D. H. .. *Jour. of Geo.*, 1954, **62**, 1.

Fancher, G. H. .. *Texas Res. Comm.*, 1950, Bulletin No. 4.

Hughes, D. S. and Cooke, C. E. *Geophysics*, 1953, **18**, 2.

Tickell, F. G. .. *The Examination of Fragmental Rocks.*

Mechem, O. E. and McCurdy, R. C. *Trans. Amer. Inst. Min. Met. Eng.*, 1933, **103**, 256.

STUDIES ON PHOSPHORUS OXYCHLORIDE AND ALUMINIUM CHLORIDE COMPLEX

By K. N. Venkataraman and A. R. Vasudeva Murthy

(*Department of Inorganic and Physical Chemistry, Indian Institute of Science, Bangalore-12*)

Received December 22, 1959

(Communicated by Dr. M. R. A. Rao, F.A.SC.)

Phosphorus oxychloride has been found to be a versatile solvating liquid for many inorganic compounds. A large number of non-polar halides of the elements of III, IV and V groups of the periodic table react with phosphorus oxychloride and form complexes which are stable and easily isolated. Similarly a large number of solvates of metal oxides with phosphorus oxychloride have been reported in literature. This solvating property of the oxychloride is attributed to its co-ordinating tendency through either oxygen[1] or chlorine[2–3] acting as donor atom.

Earlier reports about the complex formed between phosphorus oxychloride and aluminium chloride indicated the complex to be of composition $AlCl_3.POCl_3$,[4] but recent observations concerning its composition are conflicting. Gutman[5] claims that the complex is $AlCl_3.POCl_3$ while Groeneveld and Zuur[6] report the complex to be $AlCl_3.2\,POCl_3$ prepared under similar conditions. The latter authors have postulated the possible existence of other complexes with the following compositions: $AlCl_3.5\,POCl_3$ and $AlCl_3.6\,POCl_3$.

The preliminary investigations of the present authors indicated that the molar ratio of aluminium chloride and phosphorus oxychloride in the complex formed was 1 : 2. A detailed investigation was therefore undertaken to throw more light on the composition of the complex and also to study its physico-chemical properties, such as its cryoscopic behaviour, electrical conductivity and absorption spectra in solution.

Experimental

Phosphorus oxychloride

Phosphorus oxychloride of C.P. quality (E. Merck) was purified by distilling in an all-glass apparatus in an atmosphere of pure and dry nitrogen. The fraction distilling between 105–106° C. (683 mm.) was collected and preserved in sealed ampules (about 2·5 g. in each). The purity of the

oxychloride was checked by the estimation of the phosphate and the chloride obtained after hydrolysing a known quantity of the sample with dilute alkali. The results indicated that phosphorus oxychloride was 99·9% pure.

Aluminium chloride

Anhydrous aluminium chloride was prepared by passing dry hydrogen chloride over heated aluminium filings (Merck A.R. quality) in a pyrex glass tube maintained at 250° C. The condensed aluminium chloride was resublimed into a series of bulbs in a current of dry hydrogen chloride. The bulbs each containing about 2–3 g. of the anhydrous chlorides were sealed off. A representative sample was analysed by hydrolysing the chloride in a dilute solution of alkali and estimating the aluminium as the hydroxy quinolate and the chlorine by Volhard's method. The analytical results showed that the anhydrous chloride was 99·8% pure.

1. *Preparation of the complex*

The method followed for the preparation of the complex was essentially the same as described by earlier workers with a few minor improvements. The transfer of materials, etc., was carried out in a 'dry' box and the experiments were conducted in all-glass vessels.

A known quantity of anhydrous aluminium chloride was taken in a dry flask fitted with a phosphorus pentoxide guard tube. A known excess of phosphorus oxychloride was introduced into the same vessel. Considerable heat was evolved during the mixing of the reagents. The anhydrous aluminium chloride dissolved slowly in the oxychloride at room temperature. The reaction could be completed within fifteen minutes by heating at 95° C. The flask was cooled to room temperature and the excess of oxychloride was then removed in two ways: (i) by passing dry air through the solution and (ii) by removing the vapours under vacuum.

(i) *Sample obtained by passing dry air.*—A portion of the solution of aluminium chloride in phosphorus oxychloride as obtained above was transferred to a dry glass bubbler assembled along with suitable traps and guard tubes. Dry air was slowly drawn through the solution (for 24–36 hours) till a free flowing powder was obtained. The free flowing powder samples (2–3 g.) were preserved in sealed tubes.

(ii) *Removal of the solvent by evacuation.*—Another portion of the homogeneous solution was transferred to an evaporating dish which was placed in a vacuum desiccator and evacuated slowly at 25° C. with occasional stirring till a free flowing powder was obtained. The powder samples were preserved in sealed tubes as mentioned above.

Analysis of the samples.—The estimation of aluminium and phosphorus in presence of each other presents some difficulties. In order to obtain reliable analytical results the method described in an earlier communication was adopted for the determination of both phosphorus and aluminium.[7] The chloride content of the samples was determined after hydrolysing the substance with a cold dilute solution of sodium hydroxide by Volhard's method. This procedure prevented any loss of hydrogen chloride during hydrolysis in water and gave correct analytical results.[8]

The analytical results indicated that a stable complex is obtained in whatever way the excess of oxychloride is removed from a solution of aluminium chloride in excess of phosphorus oxychloride. The molecular ratio of aluminium chloride and phosphorus oxychloride in the complex was found to correspond to 1 : 2.

As has been pointed out earlier, Gutman reports a complex of the composition $AlCl_3.POCl_3$. But no details of the conditions of preparation and methods of removal of the excess oxychloride are described. Under the specified conditions described above, only one type of complex can be isolated corresponding to the composition $AlCl_3.2\ POCl_3$. The physico-chemical properties of the complex are described below.

2. *Cryoscopic behaviour of the complex in nitrobenzene*

Preliminary investigations indicated that nitrobenzene was the most suitable solvent for the cryoscopic work. The solubility of the complex in nitrobenzene at 25° C. was determined and this corresponded to the value 5·91 g. in 100 g. of nitrobenzene[9] whereas other organic solvents like carbon tetrachloride, benzene, etc., could dissolve both aluminium chloride and phosphorus oxychloride separately but the complex was found to be insoluble in such solvents. Therefore all the cryoscopic measurements were carried out in nitrobenzene solutions only.

Preparation of pure and dry nitrobenzene.—Nitrobenzene (C.P. quality) was purified by the method similar to that described by Meisenheimer and Dorner[10] and Roberts and Bury.[11] A pure sample of nitrobenzene was distilled and the middle portion was fractionally crystallised three times, dried over anhydrous calcium chloride and again distilled. The middle portion was stored over phosphoric anhydride and just before commencing the experiment was distilled at 10 mm. pressure into cryoscopic tubes. A carefully dried all-glass distillation apparatus was used for such purposes. The freezing point of such a sample was 5·77° C. $\pm$ 0·005.

The purity of nitrobenzene and its cryoscopic constant (K_f) were checked by determining the molecular weight of resublimed naphthalene which is

known to be a monomer in this solvent.[11] K_f of nitrobenzene was taken to be 6·89[11] which is in good agreement with the value calculated using latent heat of fusion of nitrobenzene as 22·46 cal./g. as determined by Meyer.[12]

The molecular weights of anhydrous aluminium chloride, and phosphorus oxychloride as well as that of the complex were determined separately and the following values were obtained:

Aluminium chloride: Mol. weight in nitrobenzene		$134·6 \pm 1$
Phosphorus oxychloride	,,	$163·7 \pm 3·5$
"Complex"	,,	$345·6 \pm 5$

It has been observed that aluminium chloride has the formula Al_2Cl_6 up to 400° C. corresponding to all the three states of aggregation.[13] The molecular weight of aluminium chloride in solutions of liquids like carbon disulphide, benzene, etc., also corresponds to the dimeric form; whereas in solvents like pyridine[14] and ether[15] the anhydrous chloride is essentially monomeric. In general, it has been claimed that in any solvent that is known to combine with anhydrous aluminium chloride, aluminium chloride has a molecular weight corresponding to $AlCl_3$.

Aluminium chloride forms an addition product with nitrobenzene also[16] with the formula ($AlCl_3.C_6H_5NO_2$). The molecular weight of anhydrous aluminium chloride as determined in the present experiment indicates that it is in monomeric form in nitrobenzene solution at comparatively low concentrations. This result is in agreement with the values reported in literature.[17]

Phosphorus oxychloride has a molecular weight in nitrobenzene corresponding to the monomeric form. While at higher concentrations there seems to be a tendency towards dimerisation. However, the values obtained in the present investigation agree better with the theoretical value than reported earlier.[18]

The determination of the molecular weight of the complex formed between phosphorus oxychloride and anhydrous aluminium chloride in nitrobenzene has been carried out using comparatively dilute solutions. In spite of this the value obtained in the present investigation (345·6) is far from the theoretical value corresponding to the molecular formula $AlCl_3.2\,POCl_3$ (440·1). This deviation of the experimental value from the theoretical value may be attributed to the dissociation of the complex at low concentration into phosphorus oxychloride and a lower complex in the following

way: $AlCl_3.2\ POCl_3 \rightleftharpoons AlCl_3.POCl_3 + POCl_3$. One may even expect the complete breakdown of the complex into aluminium chloride and phosphorus oxychloride thus giving rise to three molecules instead of two molecules as suggested in the foregoing. A comparison with the complexes formed between zirconium and hafnium tetrachlorides with phosphorus oxychloride eliminates the probability of getting three molecules.[19]

3. *Electrical conductivity in nitrobenzene*

In order to ascertain whether the complex corresponding to the molecular composition of the solid existed in solution, electrical conductivity measurements of the complex in nitrobenzene solution were carried out. A modified form of Freas conductivity cell was used. The electrodes consisted of two circular platinum plates (diameter $\frac{3}{4}''$) kept apart at a distance of 2 mm. The conductivity cell had an all-glass airtight lid in order to protect the solution from contamination with atmospheric moisture. The measurements of conductivity were carried out with the help of "Electrospezial" conductivity meter (Model GM 4249). The conductivity cell was kept in a thermostat at $25 \pm 0{\cdot}05°$ C.

The electrodes were platinised and the cell constant was determined in the usual manner. The cell constant had a value of 0·03865 which enabled the measurement of conductivity of the low conducting non-aqueous solutions. The nitrobenzene used had a specific conductivity of $0{\cdot}6 \times 10^{-7}$ mhos per cm. at 25° C. and this agrees with the value given by Payne (1×10^{-7} mho per cm.).[10, 11, 20]

Aluminium chloride in nitrobenzene had a specific conductivity of 4×10^{-5} mhos/cm. at a concentration of 0·01 mole per litre which increased to $148{\cdot}7 \times 10^{-5}$ mhos with increase in concentration to 1·01 mole per litre. Similarly the specific conductivity of phosphorus oxychloride solution in nitrobenzene increased from $1{\cdot}69 \times 10^{-6}$ mhos/cm. to $25{\cdot}43 \times 10^{-6}$ mhos when the concentration was increased from 0·02 mole/litre to 2·13 moles/per litre. These results are presented graphically in the curves A and P of Fig. 1. These experimental values are in agreement with the results reported in literature.[18, 21]

The electrical conductivity of different mixtures of aluminium chloride and phosphorus oxychloride in nitrobenzene prepared by mixing the individual components to give suitable molar ratios at different concentrations were measured. The change in conductivity of the mixture of the reactants in nitrobenzene while keeping the concentration of aluminium chloride complex isolated ($AlCl_3.2\ POCl_3$) were also measured.

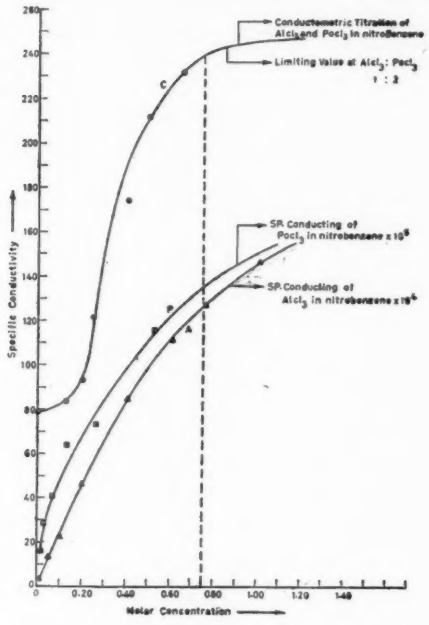

FIG. 1

It is known that anhydrous aluminium chloride conducts electricity in all the three states of aggregation except at the melting-point. The ionic species responsible for conducting the current are reported[22] to be $Al_2Cl_6 \rightleftharpoons Al^{+3} + (AlCl_6)^{-3}$. In solvents like ethyl chloride the aluminium cation is observed[23] to be heavily solvated[6] as $[Al\,(C_2H_5Cl)_n\,]^{+3}$. It is also known that in aqueous medium the aluminium ion is solvated corresponding to a co-ordination number six. From the cryoscopic data, it has already been indicated that the monomeric form of aluminium chloride, is associated with nitrobenzene but the extent of solvation is not known. It is very difficult to distinguish from the cryoscopic data whether the two particles correspond to $2\,AlCl_3$ or Al^{+3} and $(AlCl_6^{-3})$ owing to autoionisation. It is reasonable to attribute the electrical conductivity of aluminium chloride in nitrobenzene to these ionic species.

Phosphorus oxychloride is not a very good conductor in nitrobenzene when compared with aluminium chloride. Even this feeble conductance which is not very much different from the solvent itself may be attributed to the ionic species formed by the autoionisation of phosphorus oxychloride into: $2\,POCl_3 \rightleftharpoons POCl_2^+ + POCl_4^-$ as suggested by earlier workers.[18, 24]

Many of the electrolytic properties of phosphorus oxychloride have been explained on the basis of such an ionisation.

The conductivity of various mixtures of aluminium chloride and phosphorus oxychloride in nitrobenzene in different proportions is higher than the sum of the individual conductivities of the two components calculated from the graph. For instance, the specific conductivity of a mixture of equal volumes of 0·6 M $AlCl_3$ and 0·6 M $POCl_3$ (the resulting mixture will have 0·3M $AlCl_3$ and 0·3 M $POCl_3$) was found to be $11·04\times10^{-4}$ mhos/cm. which is nearly double the value of the sum of the individual conductivities at the corresponding concentrations in solution ($6·75\times10^{-4}$ mhos for $AlCl_3$ $0·079\times10^{-4}$ for $POCl_3$ $6·83\times10^{-4}$).

In another case when equal volume of 0·4 M solution of aluminium chloride was mixed with 0·6 M solution of phosphorus oxychloride in nitrobenzene, the conductivity was found to be $12·47\times10^{-4}$ mhos/cm. Whereas the sum of the conductivities of individual components corresponding to 0·2 M aluminium chloride and 0·3 M phosphorus oxychloride is equal to $4·78\times10^{-4}$ mhos/cm.

Similar observations are made in other cases also. It can be inferred from the above results that the contribution of phosphorus oxychloride to the electrical conductivity is very small when compared with that of aluminium chloride. However, the mixture shows a marked increase in the conductivity indicating thereby the conducting species are very much different from either $AlCl_3$ or $POCl_3$.

The conductivities of the solution (Table I) prepared from the isolated complex $AlCl_3.2\,POCl_3$ in nitrobenzene also show a higher value than the sum of the conductivities of the individual components at corresponding concentrations. However, the solubility of the isolated complex,[9] which corresponds only to 0·53 molar, restricts the choice of higher concentration. Heating the mixtures of the two components in nitrobenzene solution to 95° C. had little effect on conductivity indicating that the reaction between aluminium chloride and phosphorus oxychloride on mixing was complete even at room temperature.

4. *Conductometric titration of aluminium chloride with phosphorus oxychloride in nitrobenzene*

A solution of aluminium chloride in nitrobenzene (0·37 M) was titrated against a standard solution of phosphorus oxychloride in nitrobenzene conductometrically and it was found that the specific conductivity of the resulting system attained a limiting value at a point corresponding to the

TABLE I

Electrical conductivity of the complex $AlCl_3.2POCl_3$ in nitrobenzene at 25° C.

Concentration in mole per litre $\times 10^2$	0·34	0·68	2·05	3·42	4·79	6·16	6·84
Sp. conductivity in mho./per cm. 10^4	0·01	0·27	0·98	1·53	2·04	2·69	3·18

molecular ratio of the components in solution $AlCl_3$: $POCl_3$ 1 : 2. Conductometric titration curve (C) is given in Fig. 1. This value clearly indicated the formation of the complex corresponding to a definite composition $AlCl_3.2\ POCl_3$.

It has already been pointed out that the conductivity of the complex in solution is very much higher than the sum of the conductivities of the two components at corresponding concentrations. This may be attributed to the formation of $AlCl_4^-$ and $POCl_2^+$ ions and the tendency of the additional phosphorus oxychloride to dissociate into $POCl_2^+$ and Cl^- ions. All these species are likely to bring about a perceptible increase in specific conductivity of the solutions of the complex formed between aluminium chloride and phosphorus oxychloride in nitrobenzene.

5. *Absorption spectra of the systems $AlCl_3$–$POCl_3$ in nitrobenzene*

The absorption spectrum of pure and dry nitrobenzene showed a peak at 4150 Å with an optical density of $9{\cdot}25\times10^{-2}$. This is in agreement with the value reported in literature.[26] Absolute alcohol was used as a standard while measuring the absorption of nitrobenzene. The absorption spectrum of phosphorus oxychloride in nitrobenzene, using nitrobenzene itself as a standard, did not show any characteristic absorption maximum.

Pure and dry nitrobenzene has a straw yellow colour, whereas even a dilute solution of aluminium chloride is deep yellow. The intensity of the colour depends on the concentration. The absorption maximum is found to shift towards longer wavelengths with increase in concentration. The absorption maximum changed from 4400 Å to 4620 Å when the concentration of the solution was changed from 0·02 M to 0·4 M. Beer's law was found to be valid between concentrations 0·016 M and 0·025 M of aluminium chloride in nitrobenzene at a wavelength of 4400 Å. The optical density of aluminium chloride solution in nitrobenzene reached a limiting value of 0·825 at 0·22 M.

The optical density measurements of the mixtures containing various proportions of aluminium chloride and phosphorus oxychloride (corres-

ponding to solutions of concentration in the range where Beer's law is valid) indicated that there was another range of maximum absorption between 6950 Å and 7200 Å which is not observed in case of either nitrobenzene or the individual solutions of aluminium chloride or oxychloride. It could therefore be inferred that there was complex formation between aluminium chloride and phsophorus oxychloride when mixed in nitrobenzene solution even at room temperature.

The solutions of the isolated solid complex in nitrobenzene also exhibited a similar peak in the range 6900 Å–7200 Å. The complex whether it is formed in solution by the addition of aluminium chloride and phosphorus oxychloride in nitrobenzene or prepared separately and then dissolved in nitrobenzene appear to be the same.

SUMMARY

1. Anhydrous aluminium chloride reacts with phosphorus oxychloride to give a complex with a composition $AlCl_3.2\ POCl_3$ which can be prepared in the form of a free flowing powder.

2. The phosphorus oxychloride-aluminium chloride complex in nitrobenzene dissociates into $AlCl_3.POCl_3$ and $POCl_3$ as indicated by the cryoscopic measurements.

3. The solution of the complex in nitrobenzene has a higher specific conductivity than the corresponding electrical conductivities of individual components. Similar higher electrical conductance is observed when the two components are mixed in nitrobenzene in different proportions.

4. When a solution of anhydrous aluminium chloride in nitrobenzene is titrated conductometrically against a solution of phosphorus oxychloride in nitrobenzene, a limiting value in the conductivity is reached at point corresponding to the molecular composition, the components in the ratio of 1 : 2 $AlCl_3$: $POCl_3$ in solution.

5. The absorption maxima of the complex in nitrobenzene solution differ from the absorption maximum of the individual components.

ACKNOWLEDGMENT

The authors wish to express their grateful thanks to Professor K. R. Krishnaswami and Professor M. R. A. Rao for their keen interest in the work.

REFERENCES

1. Groenveld, W. L. .. *Rec. Trav. Chim.*, 1956, **75,** 594.
2. Gutman, V. .. *Ibid.*, 1956, **75,** 603.
3. Payne, D. S. .. *Ibid.*, 1956, **75,** 620.
4. Casselmann, W. .. *Ann. Chem.*, 1852, **83,** 257; 1856, **98,** 213.
5. Gutman, V. .. *Z. anorg. allgem. Chem.*, 1952, **269,** 279.
6. Greenveld, W. L. and Zuur, A. P. *Rec. Trav. Chem.*, 1957, **76,** 1005.
7. Venkataraman, K. N. and Vasudeva Murthy, A. R. *Jour. Sci. and Ind. Res.*, 1959, **18 B**, No. 12, 537–539.
8. Larsen, E. M., Howatson, J., Gammill, A. M. and Wittenberg, L. *J. Am. Chem. Soc.*, 1952, **74,** 3489.
9. Venkataraman, K. N. and Vasudeva Murthy, A. R. *Curr. Sci.*, 1958, **27,** 389.
10. Meisen Heimer, J. and Dorner, O. .. *Ann. Chem. Justus Liebys*, 1930, **482,** 130.
11. Roberts, H. M. and Bury, C. R. *J. Chem. Soc.*, 1923, 2037.
12. Meyer, J. .. *Z. Physick. Chemie.*, 1910, **72,** 245.
13. Friedel, C. and Crafts, J. M. *Compt. rend.*, 1880, **106,** 1764.
14. Werner, A. .. *Z. anorg. Chem.*, 1897, **15,** 1.
15. Beckmann, E. .. *Z. Physick. Chem.*, 1903, **46,** 860.
16. Menschutkin, B. .. *J. Rus. Phy. Chem. Soc.*, 1910, **42,** 58.
17. Kohler, E. P. .. *Am. Chem. Jour.*, 1900, **24,** 385.
18. Dadape, V. V. and Rao, M. R. A. *J. Am. Chem. Soc.*, 1955, **77,** 6192.
19. Larsen, E. M. and Wittenberg, L. J. .. *Ibid.*, 1955, **77,** 5850.
20. Payne, D. S. .. *J. Chem. Soc.*, 1953, 1052.
21. Plotinikov, V. A. and Vaisberg, R. G. *Mem. Inst. Chem. Ukrain Acad. Sci.*, 1936, **3,** 337.
22. Biltz, W. and Voigt, A. .. *Z. anorg. Chem.*, 1923, **126,** 39.
23. Uschakow, M. I. .. *Ibid.*, 1929, **183,** 144.
24. Gutman, V. .. *Monatsh*, 1952, **83,** 169.
25. ————. .. *Z. anorg. u. allgem. Chem.*, 1952, **267,** 279.
26. Davis, T. L. and Heggie, R. *J. Am. Chem. Soc.*, 1935, **57,** 1622.

THERMAL STUDIES OF CLAY MINERALS FROM SOME SEDIMENTARY FORMATIONS OF ANDHRA PRADESH

By B. B. G. Sarma

(Department of Geology, Andhra University, Waltair)

Received February 4, 1960

(Communicated by C. Mahadevan, F.A.SC.)

Introduction

The study of clay minerals is of comparatively recent origin in the development of geological sciences. On account of the importance of those minerals in agriculture, construction engineering, and also in ceramic, rubber, paper and petroleum and other industries, considerable information has been gathered. Recent and modern research techniques like X-ray, Differential Thermal Analysis, Electron Microscopy and Infra-red Spectroscopy have opened new vistas for fundamental study.

The clay materials available for study are mainly of two kinds—recent clays, unconsolidated or in the process of consolidation, and ancient clays from the sedimentary formations of the geological past. In the case of the former, the environment of deposition is readily known. The environment of ancient sedimentary clays can be ascertained by other petrographic methods. A critical study of the clay minerals with reference to their environment of formation, and the changes that are brought about by the later processes of diagenesis and lithification, will be interesting. The present investigation is an attempt at the study of clay minerals from their environmental point of view. In this paper, the results of Differential Thermal Analysis of eleven clay mineral extracts from shales and shaly sandstones belonging to the Chintalapudi formation, equivalent to the Kamthis of Triassic age, from the Lower Gondwanas of Krishna District and parts of West Godavari District, in Andhra Pradesh, are presented.

Location and Nature of the Samples

The Chintalapudi formation in the Krishna District occurs as a small patch of about five square miles near Somavaram (80° 55′ ; 16° 55′). Seven of the samples are from this patch.

The other four samples are from the outcrops of the formation east of Chintalapudi (81° 3′ ; 17° 3′). The outcrops in fact form part of the Kamthi beds of Nagpur and Chanda, extending down the Godavari valley. The Somavaram and the Chintalapudi areas are removed from each other by about 15 miles and separated by khondalites. The rocks, however, bear a close resemblance and are composed of colourless or light coloured, highly friable, medium to coarse-grained felspathic sandstones and fine well-laminated shales, with intercalations of hard reddish ferruginous streaks. A number of fossil impressions of Glossopteris and Vertebraria have been described from both the areas and determine the age of the beds. The older formations in the vicinity from which the Chintalapudi formation could have derived their material, are quartzo-felspathic, sillimanite gneisses and schists and quartzites of the khondalite suite.

Experimental Procedure

All the samples were crushed and the coarse fraction separated by sieving. After dispersal in 0·01 N Sodium hexametaphosphate solution for a few days, a further separation was carried out by wet seiving using a phosphor-bronze sieve. Finer fractions were obtained by settling methods.

The Differential Thermal Analysis apparatus used is of a portable type and the results are qualitative. The instrument consists of two junctions of a differential thermocouple made of chromel : alumel, placed symmetrically in two holes of a metal crucible block and connected to a sensitive galvanometer, and a pyrometer connection placed in the same block at right angles to the line joining the thermocouple junctions. The substance to be studied and calcined alumina, which is taken as the inert substance, are packed round the two junctions. The whole crucible is heated by an electrical furnace, its rate of rise in temperature being controlled by a variable resistance. Sufficient care is taken to see that uniformity in nature of packing and in rate of rise of temperature at 15° C. per minute are maintained.

The instrument was initially calibrated with pure quartz powder. The difference between the ideal inversion temperature of quartz (573° C.) and the temperature at which inversion actually took place, under the existing conditions as recorded by the pyrometer of the instrument, was found to be 20° C. and is applied as a correction to all the pyrometer readings.

Results

As can be seen from the differential thermal curves shown in Figs. 1 and 2, samples 1–7 show an initial endothermic peak between 75° C. and 150° C., another between 500° C. and 620° C, and an exothermic reaction at 920° C,

Samples Nos. 2, 4, 5 and 7 show, besides, double peaks in the second endothermic trough. Samples Nos. 8, 9, 10 and 11 are similar in their behaviour to the previous ones, except for the absence of the initial endothermic peak.

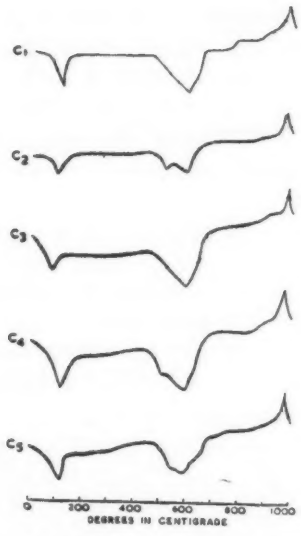

FIG. 1. D. T. A. Curves.

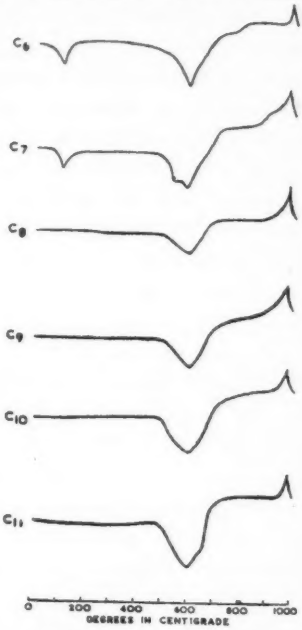

FIG. 2. D. T. A. Curves.

The curves obtained are compared with standard curves of different clay minerals given by Grim and Rowland (1942) and Kerr and Kulp (1948). The samples studied correspond very closely with minerals of the kaolinite group. The minor variations noted may be due to the occurrence of the clay minerals as mixtures and due to the presence of some impurities like sericite.

DISCUSSION

Frederickson (1952) points out that kaolinite characteristically develops in an acid environment. Millot (1952), who has analytically studied some sedimentary clays with reference to their environment of deposition, comes to the conclusion "Kaolinite sediments are due to the decomposition of crystalline rocks during the weathering. The rock must have been crystalline, because the waters that come from a mountain range covered by a sedimentary carapace are basic and are unfavourable to the formation of kaolinite. Carbonates are completely absent which is a useful criterion".

Grim, Dietz and Bradley (1949), based on their work on the Pacific sediments, point out that kaolinite is lost during marine diagenesis, but add that clay mineral investigations of recent and ancient sediments are too scanty to determine the general validity of this conclusion. However, since many definitely marine samples studied by these authors and others show illite and montmorillonite, rather than kaolinite, to be the dominant clay mineral component, an abundance of kaolinite may safely be taken to indicate a non-marine origin for the deposit containing it, in palæogeographic interpretations of an ancient sediment.

Krumbein and Sloss (1953) state that kaolinitic clay minerals are the normal end-products of podsolisation and lateritisation. There is also a tendency in this process of soil formation for leaching iron compounds.

It has been mentioned earlier that the source rocks for the Chintalapudi formation appear to be the *para*-gneisses and schists of the khondalite suite of rocks. The author has observed that, in the areas under consideration, the felspar content of the gneisses and schists is comparatively more than in some other khondalite areas. Weathering of these would have yielded the kaolinitic group of clay minerals. The presence of plant fossils to the entire exclusion of marine fossils can also be taken as an evidence for continental conditions of deposition. The streaks of ferruginous matter occurring as intercalations in the Chintalapudi formation are probably the result of the natural tendency for leaching of the iron compounds under podsolisation.

Size analysis of the Chintalapudi samples indicates variations in the sorting of sediments. There is better sorting towards the centre of the patch of the formation compared to the marginal areas. This is generally true in the case of lakes.

Conclusions

The Chintalapudi samples studied show the presence of the kaolinite group of clay minerals. Though the samples are from two different areas, there is a consistency in the clay mineral composition. It may be concluded that the formation was deposited under non-marine conditions, possibly in a lacustrine or fluvio-lacustrine environment. X-ray data, which will be presented elsewhere, confirms the identification of the minerals.

Summary

Eleven clay mineral extracts from shales and shaly sandstones equivalent to Kamthis of Triassic age, from the Somavaram (80° 55′ ; 16° 55′) and Chintalapudi (81° 3′ ; 17° 3′) areas, are studied by Differential Thermal

Analysis. The presence of kaolinite group of clay minerals is indicated. The kaolinites would have formed by the erosion of the *para*-gneisses and schists, which are the source rocks for the Chintalapudi sandstones, and are suggestive of deposition under continental conditions, possibly in a fluvio-lacustrine environment.

ACKNOWLEDGEMENTS

The author is grateful to Professor C. Mahadevan for guidance and criticism, and to the Council of the National Institute of Sciences of India for the award of a Junior Research Fellowship to carry out this work.

REFERENCES

Frederickson, A. F. .. "Symposium on Problems of clay and laterite genesis," *A.I.M.E.*, 1952, 1–11.

Georges Millot .. "Symposium on problems of clay and laterite genesis," *Ibid.*, 1952, 107–14.

Grim, R. E., Dietz, R. S. and Bradley, W. F. *Geol. Soc. Am. Bull.*, 1949, **60**, 1806–07.

——— and Rowland, R. A. .. *Am. Min.*, 1942, **27**, 746–61.

——— .. *Ibid.*, 1942, **27**, 801–18.

Kerr, P. E. and Kulp, J. L. .. *Ibid.*, 1948, **33**, 387–419.

Krumbein, W. C. and Sloss, L. L. *Stratigraphy and Sedimentation*, W. H. Freeman & Co., San Fransisco, 1953, 150–52.

432–60 Printed at the Bangalore Press, Bangalore City, by T. K. Balakrishnan, Superintendent and Published by The Indian Academy of Sciences, Bangalore

NOTICE TO AUTHORS

Scientific papers intended for publication in the *Proceedings of the Indian Academy of Sciences* can be accepted only when they are communicated by a Fellow of the Academy whose duty shall be to satisfy himself that such communications are fit to be read at the Meeting of the Academy and published in its *Proceedings*.

Papers should not ordinarily exceed fifty pages of foolscap. MSS. should be either typewritten or written in legible hand on one side of the paper. All papers should be carefully revised by the authors and should be absolutely in final form for printing. Position for text-figures should be indicated. Each paper shall conclude with a critical summary not exceeding 350 words.

Drawings, diagrams or other illustrations should be made on larger scale (preferably) twice the size than the ones in which they are intended to appear. They should be done in Indian ink on bristol board with lettering in pencil. Scale of magnification of camera lucida tracings should be indicated by the side of drawings. In certain special cases arrangements will also be made for monochrome lithographic and other colour plates. Reduction of illustrations desired should be indicated in pencil. Appropriate legends should accompany all drawings. Names of authors are to be marked in pencil on the left-hand corner of drawing sheets. Photomicrographs should be securely mounted with colourless paste.

All tables, quotations and footnotes which will be set hereafter (beginning from Vol. I, No. 2) in types smaller than the text, should be typewritten on separate sheets and placed with the text in proper sequence. Footnotes should be numbered in Arabic numerals.

References to literature in the text should be given, whenever possible, in chronological order, only the names of authors and years of publication, in brackets, being given. They should be cited in full after the summary, the authors' names following in alphabetical order. Thus,

Name or Names of author; Name of Journal (abbreviation) with a single underline; Year of publication; Number of Volume with a double underline, and lastly page. The following would be a useful illustration:—

Bergmann and Stather . . . . . Z. Physiol. Chem., 1926, 152, 189.

Two copies of slip-proof and wherever possible, a page proof for final revision will be sent to authors. All corrections are best made on the slip-proof which should be transmitted to the Office of the Academy. All proof corrections involve heavy expenses which would be negligible if the papers are carefully revised by the authors before submission.

Fifty free reprints including plates and with cover will be supplied for each paper. Additional copies can be supplied at cost on previous intimation.

Blocks appearing in the *Proceedings* will be available for purchase by their respective authors. Orders for the same should be sent along with the corrected proofs and in any case not later than one month after the date of publication of the paper. The price charged would be 25% of the actual cost of the blocks *plus* freight and despatching charges. If the blocks are reproduced in other journals or publications, due acknowledgment should be made in them to the *Proceedings*.

The original drawings and plates of blocks appearing in the *Proceedings* will be returned to such of the authors as may require them provided the cost of despatching such originals is borne by them.

CONTENTS

PAGE

Equations of Sky Components with a " C.I.E. Standard Overcast Sky " . . . . . **T. N. Seshadri** 233

Proton Emission from Nuclei Due to Neutron Interactions . . . . . **G. S. Mani and K. G. Nair** 243

Thermal Diffusivity of a Roof Slab from *in situ* Temperature Measurements . . . . . **B. C. Raychaudhuri** 258

A Simple Method for Measuring Porosity in Rocks . . . . . **S. Balakrishna and G. Shankar Narayana** 265

Studies on Phosphorus Oxychloride and Aluminium Chloride Complex . . . . . **K. N. Venkataraman and A. R. Vasudeva Murthy** 270

Thermal Studies of Clay Minerals from Some Sedimentary Formations of Andhra Pradesh . . . . . **B. B. G. Sarma** 280